THE EVOLUTION OF MASSIVE STARS

PART III. HYDROGEN EXHAUSTION THROUGH THE ONSET OF CARBON BURNING

by Chushiro Hayashi
Kyoto University

and

Robert C. Cameron
Goddard Space Flight Center

NATIONAL AERONAUTICS AND SPACE ADMINISTRATION • WASHINGTON, D. C. • DECEMBER 1962

THE EVOLUTION OF MASSIVE STARS

PART III. HYDROGEN EXHAUSTION THROUGH THE ONSET OF CARBON BURNING

By Chushiro Hayashi
Kyoto University
Kyoto, Japan

and

Robert C. Cameron
Goddard Space Flight Center
Greenbelt, Maryland

NATIONAL AERONAUTICS AND SPACE ADMINISTRATION

For sale by the Office of Technical Services, Department of Commerce,
Washington, D.C. 20230 -- Price $1.25

THE EVOLUTION OF MASSIVE STARS, PART III. HYDROGEN EXHAUSTION THROUGH THE ONSET OF CARBON BURNING

by
Chushiro Hayashi
Kyoto University
and
Robert C. Cameron
Goddard Space Flight Center

SUMMARY

Computations are made for the evolution of a population I star of 15.6 solar masses and an age-zero composition of hydrogen concentration X = 0.90, helium concentration Y = 0.08, and the concentration of the remaining elements Z = 0.02, through four phases: (1) hydrogen exhaustion in the convective core, (2) gravitational contraction of the core, (3) helium burning, (4a) the onset of carbon burning, (4b) the onset of neon burning in the absence of a preceding carbon burning phase. This discussion builds upon the model treated by Sakashita, Ono, and Hayashi. It is assumed there is no mass loss from the stellar surface, no mixing except in the convective core, and the opacity of the star is due entirely to electron scattering. Radiation pressure is taken fully into account.

The hydrogen exhaustion phase is taken to begin when $X_{core} = 0.02$. The effective temperature increases slightly for 1.4×10^5 years while hydrogen burning in the core gradually ceases to be effective. When the energy sources which are due to gravitational contraction and hydrogen burning in a thin shell at the core boundary become important (simultaneously), the envelope begins to expand rapidly.

The time spent in helium burning, 1.2×10^6 years, is about 1/14 of that spent in hydrogen burning. Helium burning accounts for the early-type supergiant branch of luminous galactic clusters such as h and χ Persei.

Preliminary results have been obtained for the onsets of the carbon and neon burning phases. The very large stellar radii obtained will be reduced considerably when the surface convection zone has been taken into account. However, the quantities which characterize the inner structure will not differ significantly from those given here.

Carbon and neon burning and more advanced phases, which have a total lifetime of the order of 10^6 years, probably account for the M-type supergiant branch of h and χ Persei and similar clusters.

CONTENTS

THE EVOLUTION OF MASSIVE STARS, PART III. HYDROGEN EXHAUSTION THROUGH THE ONSET OF CARBON BURNING*

by

Chushiro Hayashi†

Kyoto University

and

Robert C. Cameron

Goddard Space Flight Center

INTRODUCTION

The Hertzsprung-Russell (H-R) diagram of highly luminous galactic clusters, such as h and χ Persei, exhibits a wide Hertzsprung gap between early- and late-type supergiants. For clusters whose brightest stars are less luminous, the gap is narrower; it finally disappears in a cluster having a brightness equal to or less than that of the cluster M67. Cepheid variables are found in this gap, but their internal structure, their energy sources, and the cause of their pulsation are not well known. In a star's lifetime many kinds of nuclear reactions, beginning with hydrogen burning and ending with the formation of iron nuclei, are expected to occur successively in its central regions (Reference 3). Most of the late-type giants in M67 are still in the hydrogen burning phase (Reference 4), but there seems to exist a conspicuously different situation in the evolution of massive stars — for example, those in h and χ Persei.

In order to interpret the H-R diagram of luminous clusters, we will examine a population I star of mass M equal to 15.6 times the solar mass ($M_\odot$) and an age-zero composition of hydrogen concentration X = 0.90, helium concentration Y = 0.08, and the concentration of the remaining elements Z = 0.02. We shall choose this composition as representative of massive stars, and consider the evolutionary progress of this model, from hydrogen exhaustion in the core through the onset of carbon burning, in detail. Additionally, we shall study a special case, the onset of neon burning in the absence of a preceding carbon burning phase.

*This is the third part of a series. (The first two parts are listed in References 1 and 2.) A similar article by these two authors appears in the *Astrophys J.*, Vol. 136 No. 1, July 1962.

†The main part of the research for this paper was conducted while Dr. Hayashi was associated with Goddard Space Flight Center as a recipient of the National Academy of Sciences–National Research Council Post-Doctoral Resident Research Associateship. However, he also wrote part of the report after he returned to the Department of Nuclear Science at Kyoto University.

The following assumptions will be made: (1) There is no outflow of matter from the stellar surface; (2) there is no mixing of chemical components except in the convective core; (3) the star's opacity is due to electron scattering alone; and (4) the inclusion of the surface convection zone is not necessary. Assumption 3, which simplifies the computations considerably, is valid except for a shallow surface region. Assumption 4 leads to spurious values for the stellar radius in the carbon and neon burning phases; otherwise it is sufficiently valid.

A considerable amount of research has been conducted concerning the evolution of massive stars in their hydrogen burning phase (References 1 and 5-10). The present report is an extension of the work of Sakashita, Ono, and Hayashi (Reference 1), who computed a sequence of five hydrogen burning stages in which the central hydrogen content of the star in question was depleted from 0.90 to 0.06. This paper discusses four evolutionary phases:

Hydrogen exhaustion—This phase is taken to begin when $X_{core} = 0.02$. As hydrogen is consumed in the core, the mass of the convective region continues to decrease and energy generation in the core which is due to hydrogen burning is gradually replaced by gravitational energy production. At the same time, an energy source which is due to hydrogen burning in a thin shell at the core boundary becomes increasingly important. This phase terminates when central hydrogen burning becomes negligible.

Gravitational contraction— In this phase more gravitational energy is released, predominantly in the dehydrogenized core. The amount of hydrogen depletion in the aforementioned shell source is small, because of the very short time scale of this phase. Eventually the central temperature becomes sufficiently high for helium burning to occur. The gravitational contraction phase ends when the energy generation which is due to helium burning becomes comparable to that which is due to the gravitational contraction.

Helium burning— In this phase there are two nuclear energy sources: helium burning at the center and continued hydrogen burning in a shell at the boundary of the dehydrogenized region. The stellar structure is illustrated in Figure 1. In this paper the work of Hayashi, Jugaku, and Nishida (Reference 2) on helium burning is reconsidered and extended by taking into account the change of mean molecular weight μ in the convective core which is due to the conversion of helium into carbon. We find higher central temperatures for the later stages of helium burning, and when $Y_{core} = 0.35$ there is a reversal of direction of the evolutionary track in the H-R diagram from left to right (Figure 2, point e).

Carbon and neon burning— Omitting the short-lived gravitational contraction phase following helium exhaustion in the core, we will consider the hypothetical onset of pure carbon burning, and of pure neon burning in the absence of a preceding carbon burning phase. In

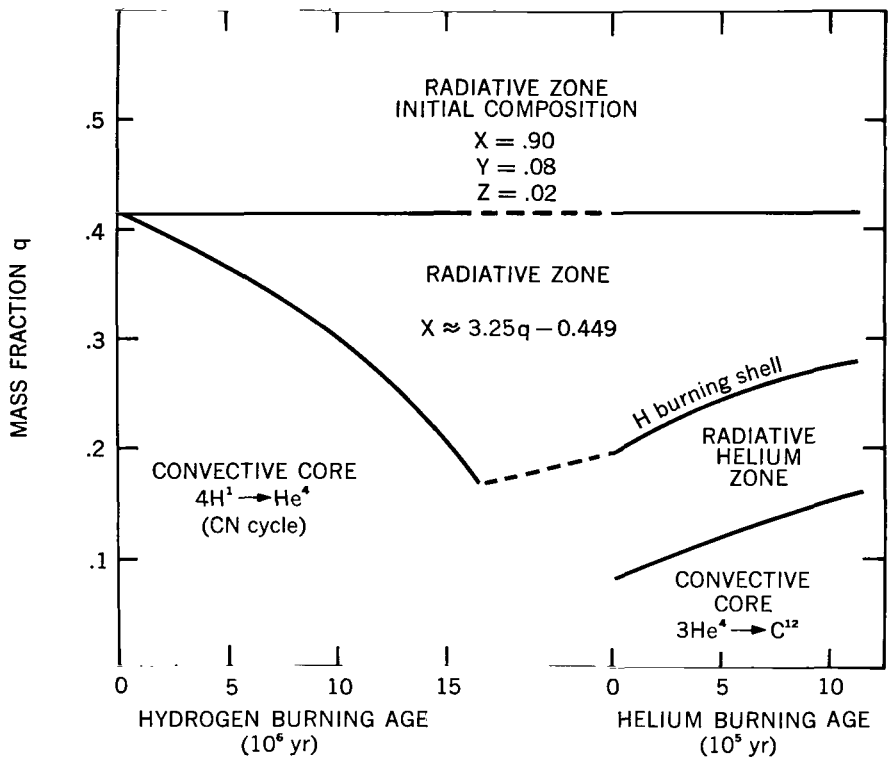

Figure 1 — Evolution of a star of mass $M = 15.6\ M_{\odot}$, during hydrogen burning (Reference 1) and helium burning. The radiative zone retaining the initial composition extends to $q = 1$.

these cases, either carbon or neon is burning in the central region. There are, from the center outward, a radiative carbon (or neon) zone, a helium burning shell, a radiative helium zone, a hydrogen burning shell, an inhomogeneous radiative zone, and a radiative zone retaining the age-zero composition. Only preliminary results have been obtained from studies of this phase. Very large stellar radii were derived, indicating the existence of a surface convection zone, as would be anticipated. This zone is not expected to appreciably affect the quantitative results obtained for the inner structure.

For computational purposes the star has been divided into two regions: an envelope, which is always in radiative equilibrium, and a core. Each of these two may consist of more than one well-defined zone. Solutions for both regions were computed on an IBM 704 or IBM 7090 electronic computer. Fitting of the solutions was accomplished by using a desk computer. The positions of the interfaces were chosen as follows: (1) at $q = 0.298$ in the hydrogen-exhaustion phase; (2) at the hydrogen burning shell in the gravitational contraction phase; (3) at the edge of the convective core in the helium burning phase; and (4) at the helium burning shell in the carbon and neon burning phases.

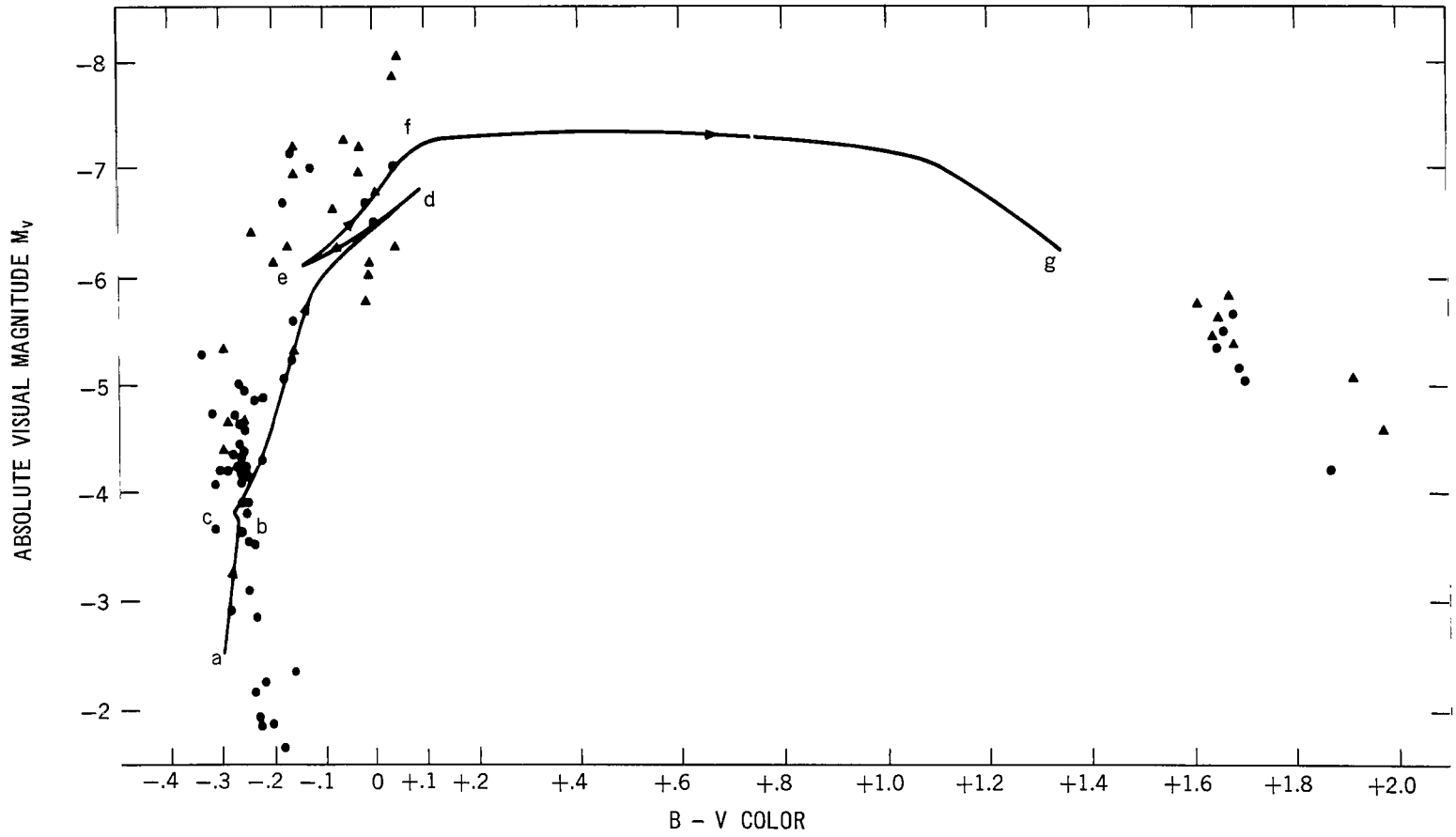

Figure 2 — The evolutionary track of a star of mass M = 15.6 $M_\odot$ with age-zero composition $X_e = 0.90$, $Y_e = 0.08$, where e indicates the outer envelope, and $X_{CNO} = 0.02/3$, superimposed on the color-magnitude diagram of the brightest stars of h and χ Persei (cf. Figure 6). X_{CNO} indicates the concentration of carbon, nitrogen, and oxygen. Segments of the track corresponding to successive evolutionary phases are identified as follows: a-b, hydrogen burning (Reference 1); b-c, hydrogen exhaustion (Figure 7); c-d, gravitational contraction; and d-g, helium burning. The evolutionary time scale derived for segments b-d and f-g is short in comparison to that of the rest of the track. Point d corresponds to the onset of helium burning in the gravitational contraction phase (Table 2 footnote); points e, f, and g correspond to stages 4, 6, and 7 of Table 3, respectively. The onset of carbon burning cannot be shown because of the uncertainty in the stellar radius during that phase. Circles represent stars within 23' of arc of either nucleus (cluster separation is about 25' of arc); triangles include stars out to 4.°0. Within the specified angular distances the stars plotted represent, in general, only a sampling (but see section entitled "Discussion", page 30). The suggestion of a gap in both coordinates, which appears in this diagram, between the upper main-sequence stars and the early supergiant branch, is to be expected, according to our results. The clusters NGC 330 and NGC 458 in the Small Magellanic Cloud show the gap more clearly (References 11 and 12).

DEFINITIONS AND BASIC EQUATIONS

The structural subscripts used in this report include: e to indicate the outer envelope with age-zero composition, b its lower boundary, 1 the hydrogen burning shell, 2 the helium burning shell, f the interface between the radiative region and the convective core, and c the center. The letter e or i is added to 1, 2, or f to indicate the external or internal side of an interface, if it is necessary to indicate this. We distinguish between $\log x \equiv \log_{10} x$ and $\ln x \equiv \log_e x$. In general the values of Chandrasekhar (Reference 13, Appendix I) are used for the solar mass, radius, and luminosity (but see the first footnote in Table 3).

The outer envelope of the star is assumed to retain its age-zero composition,

$$X_e = 0.90, \quad Y_e = 0.08, \quad Z_e = 0.02, \quad X_{CNO} = 0.02/3 \quad (\mu_e = 0.535) \quad , \tag{1}$$

where μ is the mean molecular weight. This may not hold true, however, for the young population I stars of our galaxy. Therefore, computations were repeated for the gravitational contraction phase, for a larger value of the helium content ($X_e = 0.61$, $Y_e = 0.37$, and $Z_e = 0.02$, corresponding to a model in which $M = 10.1\ M_\odot$), to determine the effect of chemical composition on the evolution.

Electron degeneracy has been neglected in computations for all phases. Therefore, the absorption coefficient is assumed to depend on electron scattering alone:

$$\kappa = 0.19(1 + X) \quad . \tag{2}$$

For stars of 15.6 solar masses, this approximation is reasonably accurate except in the stages when there is a low surface temperature (carbon and neon burning); then the effect of the outer convection zone may not be neglected, strictly speaking.

The rate of energy generation per gram which is due to the CNO cycle, which replaces the CN cycle at temperatures exceeding 3×10^7 °K, is given by Fowler (Reference 14):

$$\epsilon_H = 1.73 \times 10^{27} X_{CNO} X \rho T_7^{-\frac{2}{3}} \exp\left(-70.9\, T_7^{-\frac{1}{3}}\right) \quad , \tag{3}$$

where ρ is the density. In this and succeeding equations a numerical subscript n following T indicates $T \times 10^{-n}$ °K. Equation 3 was used for the hydrogen exhaustion phase, in which hydrogen burning occurs both in the central region and in an outer shell. In other phases the following approximation was used:

$$\epsilon_H = \epsilon_H^\circ X_{CNO} X \rho \left(\frac{T}{T_o}\right)^s \quad , \tag{4}$$

where

$$\epsilon_H^\circ = 3.14 \times 10^7, \quad T_o = 4 \times 10^7 \text{ °K}, \quad \text{and} \quad s = 14.2 \ . \tag{5}$$

The rate of energy generation during helium burning ($3He^4 \rightarrow C^{12}$), based on the data of Salpeter (Reference 15), is

$$\epsilon_{3\alpha} = \epsilon^{\circ}_{3\alpha}\, Y^3 \rho^2 \left(\frac{T}{T_o}\right)^s , \tag{6}$$

where

$$\left.\begin{aligned} \log \epsilon^{\circ}_{3\alpha} &= 35.14 - 3 \log T_o - \frac{18.76 \times 10^8}{T_o} \quad ; \\ s &= \frac{43.20 \times 10^8}{T_o} - 3 \quad , \end{aligned}\right\} \tag{7}$$

and, in this case, T_o is arbitrarily chosen so that $T/T_o \approx 1$. Recent experimental data suggest that the true value of $\epsilon^{\circ}_{3\alpha}$ may actually be smaller by a factor of 2.

As the concentration of carbon increases, the contributions from the reactions $C^{12}(\alpha,\gamma)O^{16}$ and $O^{16}(\alpha,\gamma)Ne^{20}$ to energy generation become more important. This point will be discussed in a later section ("The Helium Burning Phase," page 23). Energy generation which is due to $C^{13}(\alpha,n)O^{16}$, and the subsequent neutron capture, may be neglected since C^{13}, which is produced in the CNO cycle, can only supply stellar energy for less than 2000 years.

Nuclear reactions and the resulting energy generation involving the products of helium burning, *viz.*, carbon, oxygen, and neon, were studied by Hayashi, et al. (Reference 16), and by Reeves and Salpeter (Reference 17). The first reactions occur at about 8×10^8 °K:

$$\left.\begin{aligned} C^{12}(C^{12},p)Na^{23}, \quad Q &= 2.2 \text{ Mev} , \\ C^{12}(C^{12},\alpha)Ne^{20}, \quad Q &= 4.6 \text{ Mev} , \end{aligned}\right\} \tag{8}$$

where Q is the reaction energy. Hydrogen and helium are immediately captured by C^{12}, O^{16}, or Ne^{20}. The total energy release from each C-C reaction is about 13 Mev.

The next reaction, which occurs at about 1.1×10^9 °K, is the endothermic photodissociation of Ne^{20}, which is followed by exothermic alpha capture by Ne^{20}, Mg^{24}, etc.:

$$\left.\begin{aligned} Ne^{20}(\gamma,\alpha)O^{16}, \quad Q &= -4.8 \text{ Mev} , \\ Ne^{20}(\alpha,\gamma)Mg^{24}, \quad Q &= 9.3 \text{ Mev} . \end{aligned}\right\} \tag{9}$$

The rates of energy generation which are due to the carbon and neon burning reactions, computed by Hayashi, et al. (Reference 16), are

$$\epsilon_C = 1.0 \times 10^7 \rho X_C^2 T_9^{33.3} , \tag{10}$$

$$\epsilon_{Ne} = 6.0 \times 10^3 X_{Ne} T_9^{65.2} . \tag{11}$$

The above value of ϵ_C lies near the mean of the upper and lower values estimated by Reeves and Salpeter (Reference 17), whereas the value of ϵ_{Ne} is larger than their upper value by a factor of 100. This difference is due to their smaller value for the nuclear radius and larger value for the alpha particle width. Such an uncertainty in regard to the reaction rate of $Ne^{20}(\gamma,\alpha)O^{16}$ seems to be unavoidable at present.

Finally, energy release which is due to gravitational contraction, including the effect of radiation pressure is expressed, in general, as

$$\epsilon_g = -\frac{\partial E}{\partial t} + \frac{P}{\rho^2}\frac{\partial \rho}{\partial t}$$

$$= \frac{3kT}{2\mu H}\left(\frac{\partial}{\partial t}\ln \frac{T}{e^{\frac{8y}{3}} y^{\frac{2}{3}}} + \frac{5+8y}{3}\frac{\partial}{\partial t}\ln \mu\right) , \tag{12}$$

where

$$E\rho = \frac{3}{2}P_g + 3P_r \quad \text{and} \quad y = \frac{P_r}{P_g} = \frac{1-\beta}{\beta} , \tag{13}$$

H is the mass of a proton, and the time derivative is taken for a given mass element. P_g is the gas pressure and P_r is the radiation pressure. The total pressure P is equal to $P_r + P_g$, and $\beta = P_g/P$. In the case of the convective core, the first term inside the parentheses in Equation 12 is independent of position, and is a function only of time.

The basic equations for quasi equilibrium of the stellar interior are

$$\frac{dP}{dr} = -\frac{GM(r)}{r^2}\rho, \quad \frac{dM(r)}{dr} = 4\pi r^2 \rho, \quad \text{and} \quad \frac{dT}{dr} = \frac{1}{n+1}\frac{T}{P}\frac{dP}{dr} , \tag{14}$$

where r is the radius of the spherical part under consideration, M(r) is its mass, and G is the

universal gravitational constant. The quantity $(n+1)$ is the larger of a radiative value $(n+1)_{rad}$ and a convective value $(n+1)_{conv}$, which are defined by

$$\left.\begin{aligned} \frac{1}{(n+1)_{rad}} &= \frac{\kappa L(r)}{16\pi cG(1-\beta)\,M(r)}\ ; \\ \frac{1}{(n+1)_{conv}} &= \frac{8-6\beta}{32-24\beta-3\beta^2}\ , \end{aligned}\right\} \qquad (15)$$

where $L(r)$ is the energy production of the sphere in ergs/sec and c is the velocity of light.

In the radiative envelope, if we use the nondimensional variables defined by

$$P = p\frac{GM^2}{4\pi R^4}\ , \quad T = t\frac{\mu_e HGM}{kR}\ , \quad M(r) = qM\ , \quad r = xR\ , \quad L(r) = wL\ , \qquad (16)$$

where R is the star's radius and L is its energy production, the basic equations may be written as

$$\frac{dp}{dx} = -\frac{pq\beta l}{x^2 t}\ , \quad \frac{dq}{dx} = \frac{x^2 p\beta l}{t}\ , \quad \frac{dt}{dx} = -C\frac{pw\beta j}{t^4 x^2}\ , \quad \text{and} \quad \beta = 1 - \frac{At^4}{p}\ , \qquad (17)$$

where

$$l = \frac{\mu}{\mu_e}\ , \quad j = l\,\frac{1+X}{1+X_e}\ , \quad \text{and} \quad \frac{1}{\mu} = 2X + 0.75 + 0.56\,Z\ ; \qquad (18)$$

$$A = \frac{4\pi a}{3}\left(\frac{\mu_e H}{k}\right)^4 G^3 M^2\ , \quad \text{and} \quad C = \frac{3}{4ac}\,\frac{0.19(1+X_e)}{(4\pi)^2}\left(\frac{k}{\mu_e HG}\right)^4 \frac{L}{M^3}\ . \qquad (19)$$

In Equations 19, a is the radiation density constant. The envelope solutions are specified by one parameter, C, if the variations of X and w as functions of q are given. For the initial distribution of $X(q)$ we use the result given in Reference 1. We assume that X and w are discontinuous at the hydrogen burning shell in all phases except that of hydrogen exhaustion. The envelope solutions are determined by three parameters, C, q_1, and w_{1i}, where the subscript 1 refers to the hydrogen burning shell and the subscript i to the internal side of the interface there.

In terms of new variables,

$$\Pi = \frac{P}{P_c}\ , \quad \theta = \frac{T}{T_c}\ , \quad \phi = \frac{M(r)}{M_o}\ , \quad \text{and} \quad \xi = \frac{r}{r_o}\ , \qquad (20)$$

where

$$\left.\begin{aligned} M_o^2 &= \frac{3(1-\beta_c)}{4\pi G^3 a}\left(\frac{k}{\mu_c H}\right)^4 ; \\ r_o^2 &= \frac{3(1-\beta_c)}{4\pi G a}\left(\frac{k}{\mu_c H T_c}\right)^2 , \end{aligned}\right\} \qquad (21)$$

and subscript c refers to the center of the star, the equations of the convective core are expressed as

$$\frac{d\Pi}{d\xi} = -\frac{\Pi\phi\beta}{\theta\xi^2}, \quad \frac{d\phi}{d\xi} = \frac{\Pi\xi^2\beta}{\theta}, \quad \frac{d\theta}{d\xi} = \frac{1}{(n+1)_{conv}}\left(\frac{\theta}{\Pi}\right)\frac{d\Pi}{d\xi}, \quad \text{and} \quad \frac{1-\beta}{1-\beta_c} = \frac{\theta^4}{\Pi} . \qquad (22)$$

The solutions are specified by the parameter $y_c = (1-\beta_c)/\beta_c$. An extensive table of the necessary quantities corresponding to 21 values of $y_c = 0.0(0.025)0.5$ was computed for the convective core solutions of the helium burning, carbon burning and neon burning phases and used in the present calculations. Note that the mathematical core solution for carbon and neon burning involves also the solutions for the radiative carbon zone (attached to the convective core with constant L(r)), which are determined by specifying another parameter, such as ϕ_f, where f indicates the interface between the radiative region and the convective core.

THE HYDROGEN EXHAUSTION PHASE

The hydrogen distribution in the last stage discussed in Reference 1 is given by the formulas

$$\left.\begin{aligned} X(q) &= 0.90 && (1 \geq q \geq 0.415) , \\ &= -0.683 + 4.843\,q - 2.48\,q^2 && (0.415 \geq q \geq 0.168) , \\ &= 0.062 && (0.168 \geq q \geq 0) . \end{aligned}\right\} \qquad (23)$$

These values were adopted for the initial composition of the hydrogen exhaustion phase.

As hydrogen is consumed in this phase, the convective core shrinks and, as would be expected, complicated changes occur in the distribution of the energy sources (and also the hydrogen content); the central peak of hydrogen burning becomes lower, another peak of hydrogen burning in an outer shell becomes higher, and at the same time a broad source of gravitational energy becomes more intense.

In order to produce an evolutionary sequence of stages in the model, the hydrogen content in the center, X_c, was varied. For each of the seven stages computed, the envelope solutions — which have a fixed distribution of composition $X(q)$ given by Equation 23 — were fitted to the core solutions, at a fixed value of q, viz., $q^* = 0.298$. At greater values of q the energy sources are certainly negligible. The envelope solutions are specified by the parameter C alone. With q as the independent variable, core solutions in each stage were computed from the center out to q^*, at intervals of $\Delta q = 0.001$, by considering β_c and T_c as parameters, $X(q)$ and q_f of the previous stage being known. The details of these computations are described below. Quantities computed in the immediately previous stage will be designated by a superscript (o).

The change of hydrogen content as a function of q and t is given by

$$\frac{\partial X}{\partial t} = -\frac{\epsilon_H}{E_H} \quad \text{and} \quad \frac{\partial X_c}{\partial t} = -\frac{\int_0^{q_f} \epsilon_H \, dq}{q_f \, E_H} , \tag{24}$$

in the radiative region and in the convective core, respectively, where $E_H = 6.0 \times 10^{18}$ ergs/gm is the energy release which is due to the conversion of one gram of hydrogen into helium and f indicates the interface between the radiative region and the convective core.

If ϵ_H, given by Equation 3, is expressed by

$$\frac{\epsilon_H}{X} = A\alpha \qquad \left[A = \left(\frac{\epsilon_H}{X} \right)_c \right] , \tag{25}$$

since the change of α with time is much smaller than the changes of q_f and A, the change of $X(q)$ between the two stages considered may be written approximately, by using Equations 24, as

$$\left.\begin{aligned} \frac{\Delta \ln X}{\Delta \tau} &= -\alpha \qquad \left(q \geq q_f^{(o)} \right) , \\ &= -\omega \qquad \left(q_f^{(o)} \geq q \geq q_f \right) , \\ &= -\omega_f \qquad \left(q_f \geq q > 0 \right) , \end{aligned}\right\} \tag{26}$$

where

$$\Delta \tau = \frac{\left[A^{(o)} + A \right] \Delta t}{2 E_H} , \tag{27}$$

and

$$\left.\begin{aligned} \omega_f &= \frac{2\int_0^{q_f} \alpha\, dq}{q_f^{(o)} + q_f}, \\ \omega &= \alpha + (\omega_f - \alpha_f)\frac{q_f^{(o)} - q}{q_f^{(o)} - q_f}. \end{aligned}\right\} \tag{28}$$

The quantity ω is assumed to vary linearly with q.

The gravitational energy for this phase (see Equation 12) is expressed in the form

$$\epsilon_g = \frac{3kT}{2\mu H}\left(a_0 + a_1 q + a_2 q^2\right). \tag{29}$$

The values of the three arbitrary parameters a_0, a_1, and a_2 in the present stage are found in a first approximation by extrapolation from previous stages.

Equations 14, together with Equation 26 and

$$\frac{dL(r)}{dr} = 4\pi r^2 \rho\left(\epsilon_H + \epsilon_g\right), \tag{30}$$

are integrated from the center for input values of β_c, T_c, X_c, a_0, a_1, a_2, $q_f^{(0)}$, $A^{(0)}$, and hydrogen distribution $X^{(0)}(q_i)$, where q_i takes values from 0.002 to q^* with $\Delta q = 0.001$. The envelope is fitted to the core at $q = q^*$ with the condition that U, V, and $L(r)$ are continuous at this point. U and V are defined by

$$U = \frac{d \log M(r)}{d \log r} \quad \text{and} \quad V = -\frac{d \log P}{d \log r}. \tag{31}$$

Thus, all the physical quantities including q_f and $X(q_i)$ are determined. We then compute ϵ_g from Equation 12 and find improved values of a_0, a_1, and a_2 which give the best fit. The integrations are repeated with the new values but, at most, only a second approximation is required.

The final results of the computations are given in Table 1, where L_H and L_g are the energy production, in ergs/sec, which are due to hydrogen burning and gravitational contraction, respectively. The distribution of the energy sources is shown in Figure 3; that of the hydrogen content in Figure 4. The depletion of hydrogen in the radiative region is very small, because of the short time scale of the present phase. The evolutionary tracks in the H-R and T_c-ρ_c diagrams are shown in Figures 5, 6, and 7.

Table 1

Evolutionary Stages of a Star of Mass M = 15.6 $M_\odot$
in the Hydrogen Exhaustion Phase

$(\mu_e^2 M/M_\odot = 4.468)$

Parameter	Values at Stages 1-7						
	1	2	3	4	5	6	7
Log C	-3.009	-3.005	-3.002	-2.995	-2.989	-2.985	-2.984
Log X_c	-1.699	-2.199	-2.699	-3.199	-4.000	-4.500	-5.000
$1 - \beta_c$	0.222	0.225	0.224	0.218	0.205	0.197	0.192
Log T_c	7.653	7.683	7.713	7.737	7.757	7.762	7.764
Log ρ_c	1.102	1.195	1.288	1.379	1.473	1.510	1.526
q_f	0.158	0.154	0.148	0.127	0.081	0.051	0.028
$L_{H,core}/L$	0.99	0.97	0.91	0.73	0.24	0.09	0.05
$L_{H,shell}/L$	0.01	0.02	0.06	0.14	0.29	0.35	0.38
L_g/L	0.00	0.01	0.03	0.13	0.47	0.56	0.57
Log $R/R_\odot$	0.961	0.947	0.928	0.917	0.916	0.923	0.925
Log $L/L_\odot$	4.550	4.554	4.557	4.564	4.570	4.574	4.575
Log T_e	4.419	4.428	4.437	4.445	4.447	4.445	4.444
$t \times 10^{-5}$ (yr.)	0.000	0.940	1.235	1.332	1.359	1.362	1.363

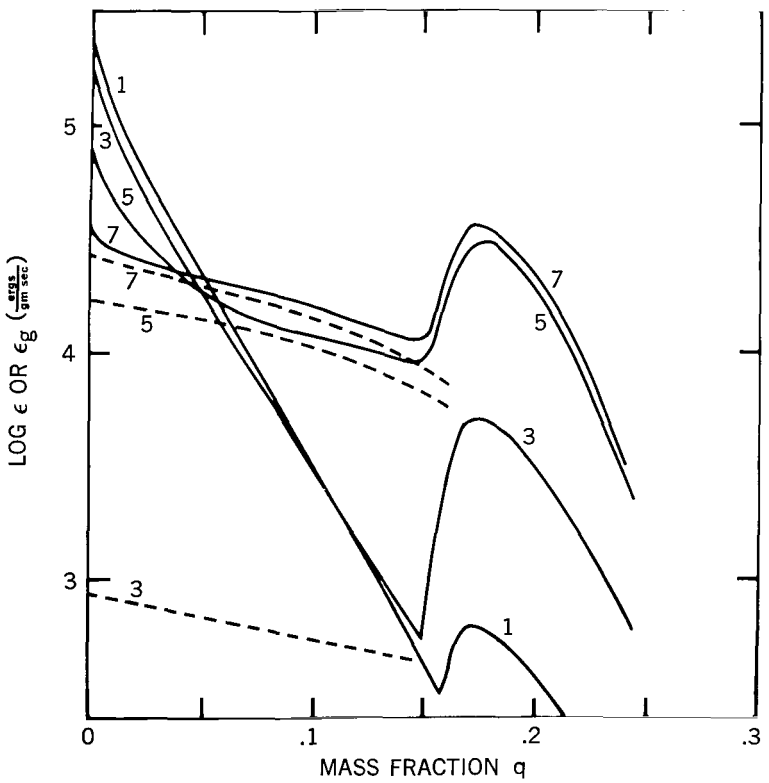

Figure 3 — Distribution of the rate of energy generation for a star of mass M = 15.6 $M_\odot$ and μ_e = 0.535, in the hydrogen exhaustion phase ($X_{core} \leq 0.02$). Solid curves give log ϵ (shell source plus gravitational energy); dashed curves log ϵ_g (gravitational energy). Numbers on the curves refer to the stages of Table 1.

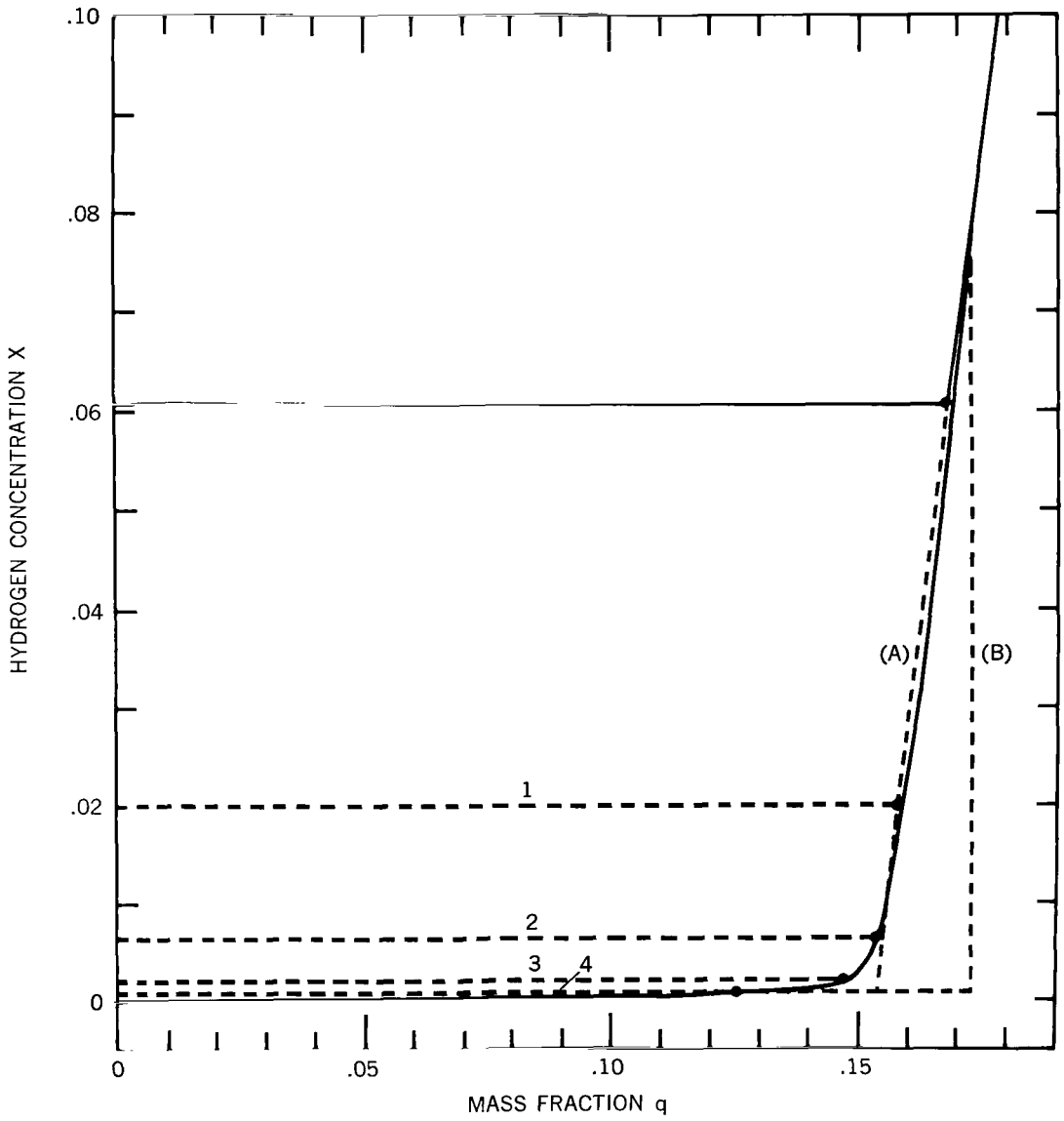

Figure 4 — Hydrogen distribution X(q) in the region of the convective core, during the hydrogen exhaustion and gravitational contraction phases for a star of mass $M = 15.6\,M_\odot$ and $\mu_e = 0.535$. Solid curves refer to the early and final stages of hydrogen exhaustion (Stage 4 in Reference 1 and Stage 7 in Table 1 of the present report, respectively). The numbers 1-4 on the curves refer to intermediate stages (Table 1). Points indicate the boundaries of the convective cores. The dashed curves A and B give the distributions assumed in cases 1 and 2 (Table 2), respectively, of the subsequent gravitational contraction phase (cf. Figure 8). Note that the line X = 0 does not coincide with the lower edge of the figure.

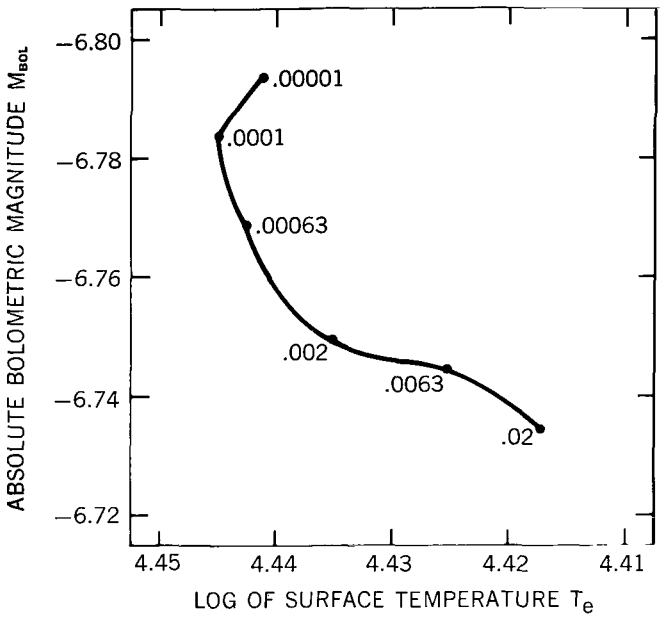

Figure 5 — Evolutionary track of a star of mass $M = 15.6\ M_\odot$ and $\mu_e = 0.535$, in the hydrogen exhaustion phase. Numbers beside the points give the hydrogen content in the core.

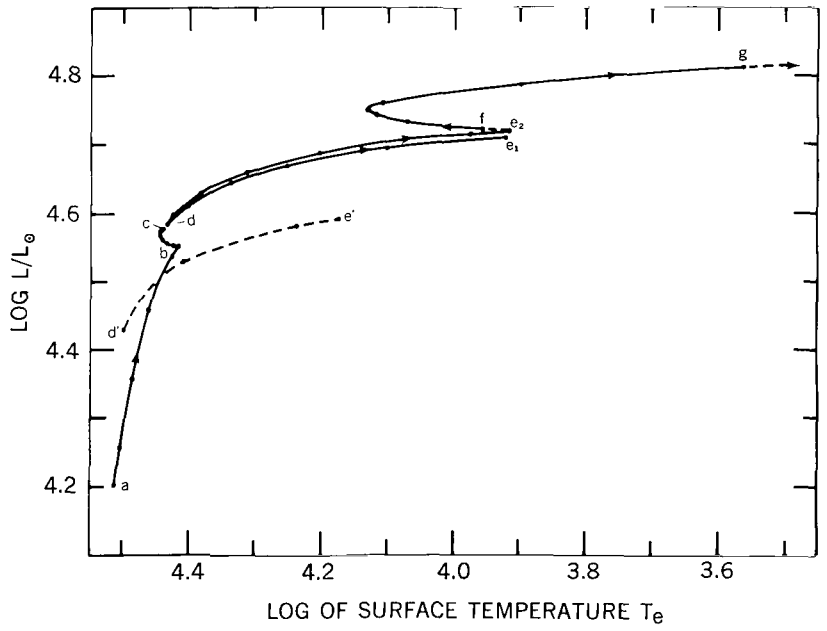

Figure 6 — Evolutionary tracks in the H-R diagram for stars of mass $M = 15.6\ M_\odot$ with $\mu_e = 0.535$ and $M = 10.1\ M_\odot$ with $\mu_e = 0.663$. In both cases $X_{CNO} = 0.02/3$ and $\mu_e^2\ M/M_\odot = 4.468$. Evolutionary phases for $M = 15.6\ M_\odot$ associated with the various segments are as follows: a-b, hydrogen burning (Reference 1); b-c, hydrogen exhaustion; d-e_1 and d-e_2, gravitational contraction up to the onset of helium burning, with $q_1 = 0.153$ (Case 1 in Table 2) and $q_1 = 0.173$ (Case 2 in Table 2), respectively; and f-g, helium burning. The segment d'-e' represents the gravitational contraction phase for $M = 10.1\ M_\odot$ (Case 1' in Table 2).

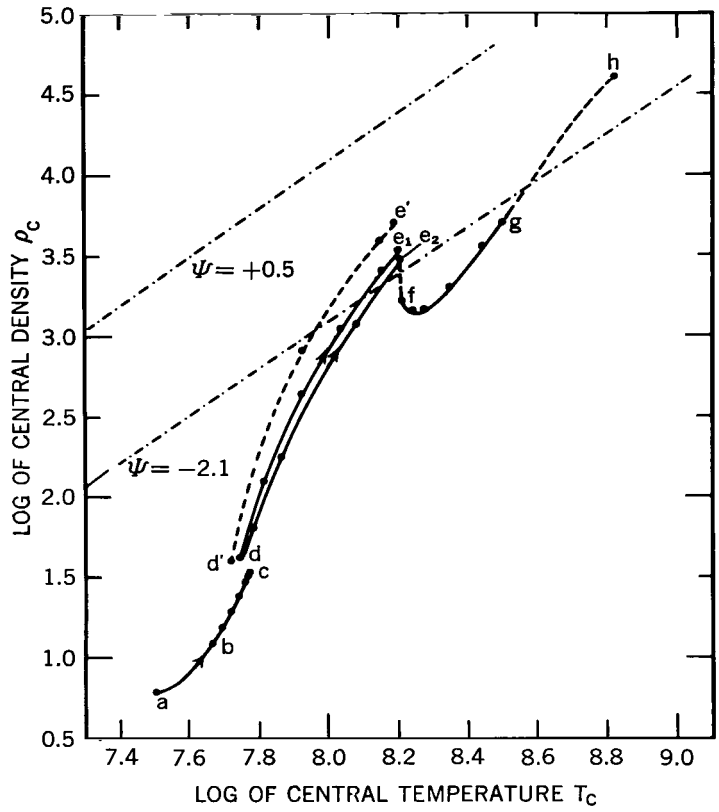

Figure 7 — Variation of central density ρ_c with central temperature T_c for stars of $M = 15.6\ M_\odot$ and $M = 10.1\ M_\odot$. Letters on the curves have the same meaning as in Figure 6. The letter "h" refers to the onset of carbon burning. Values of ψ on the broken curves indicate the degree of degeneracy (see, for example, Reference 11).

In the early stages, when L_g and $L_{H,shell}$ are small, as X_c decreases from 0.02, the central temperature increases, thus maintaining the value of $L_{H,core}$; but the change of μ_c is small, so the star contracts as a whole and moves to the left in the H-R diagram. When $X_c \approx 10^{-4}$, the temperature has become high enough for hydrogen burning to commence in an outer shell, and the envelope begins to expand as shown by the right turn in the evolutionary track (Figure 5; and Figure 2, point c).

THE GRAVITATIONAL CONTRACTION PHASE (WITH OUTER SHELL SOURCE)

The extension of the foregoing computations through the gravitational contraction phase requires many steps, since the changes in log T_c and log ρ_c are quite large even though the time scale is rather short. Results from the preceding section show that, in the present phase: (1) hydrogen burning in the central region can be neglected; (2) the depletion of hydrogen in the shell will be small; (3) ϵ_g is comparatively uniform inside the shell; and (4) the solutions regarding the rate of core contraction, and hence the gravitational energy released, will be very sensitive to the assumed input value of ϵ_g, in the following sense.

For a given stage, an input value of ϵ_g that is somewhat smaller (or larger) than the true value leads to a high (or low) value for the rate of contraction, which implies a value of ϵ_g for the next iteration that is considerably higher (or lower) than the input value. This consideration leads to the simplifying assumptions that $X(q)$ is independent of time, and that $\epsilon_g(q,t)$ is independent of q, as is also assumed by Sandage and Schwarzschild (Reference 18). These assumptions make it possible to compute the whole sequence of evolutionary stages without taking time explicitly into account. Time intervals between stages are computed from Equation 12 after the stellar structure and the values of ϵ_g are known for all stages.

The expression adopted for $X(q)$ is (cf. Equation 23)

$$\left.\begin{aligned} X(q) &= -0.683 + 4.843\,q - 2.48\,q^2 \qquad (0.415 \geq q > q_1)\,, \\ &= 0 \qquad\qquad\qquad\qquad\qquad\quad (q_1 > q \geq 0)\,, \end{aligned}\right\} \tag{32}$$

and computations will be made for two cases:

Case 1: $q_1 = 0.153$, with $X(q)$ continuous at q_1;

Case 2: $q_1 = 0.173$, with an abrupt change of X at q_1.

The objective here is to find the effect of hydrogen depletion. The value of $X(q)$ for the two cases is plotted in Figure 4, which shows that the difference between Case 1 and the last stage of the hydrogen exhaustion phase is very small (see also Figure 8). The effect of small changes in $X(q)$ on the solution of the basic equations, through its effect on μ and κ, is not large if the magnitude of X itself is small; but it is important in regard to energy generation in the shell, which is directly proportional to X.

The point q_1 is taken to indicate the location of the interface between the core (with a uniform energy source) and the envelope (with a shell source). The shell source is assumed to be thin, and its total energy generation is computed in the following way. In case 1 and in the neighborhood of q_1, we have the approximate relations

$$X = a(q - q_1) \qquad (a = 4.04)\,, \tag{33}$$

and

$$\rho T^s = \rho_1 T_1^s \left(\frac{q}{q_1}\right)^{-\gamma}\,, \tag{34}$$

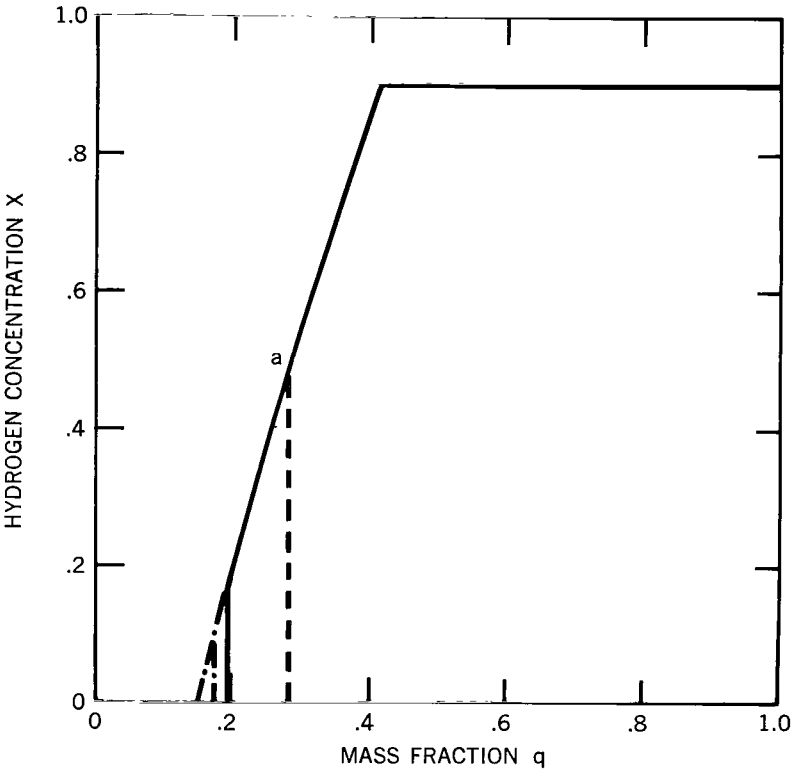

Figure 8 — Hydrogen content X as a function of the mass fraction q for a star of mass $M = 15.6\, M_\odot$ and $\mu_e = 0.535$ in the gravitational contraction and subsequent helium burning phases (cf. Figure 4). The solid curve gives the hydrogen distribution for Stage 1 of Table 3 (helium burning). The distribution is given for Stage 7 (helium nearly exhausted in the core) by the dashed curve and points to the right of point a. The two extensions of the solid curve to $q_1 = 0.153$ and $q_1 = 0.173$ give the distribution assumed in Cases 1 and 2, respectively (Table 2), of the gravitational contraction phase.

where

$$\gamma = -\left(\frac{d \log \rho}{d \log q}\right)_1 - s\left(\frac{d \log T}{d \log q}\right)_1 = \left[\left(\frac{n+s}{n+1}\right)\frac{V}{U} - \frac{d \log \mu\beta}{d \log q}\right]_1 . \tag{35}$$

Then ϵ_H, defined by Equation 4, is integrated to give

$$L_H = M \int_{q_1}^{1} \epsilon_H \, dq = \frac{M \epsilon_H^\circ X_{CNO} a q_1^2 \rho_1}{(\gamma - 2)(\gamma - 1)} \left(\frac{T_1}{T_\circ}\right)^s . \tag{36}$$

The validity of these approximations has been verified for the last stage of the hydrogen exhaustion phase by means of a comparison with the more accurate machine computations.

The core solutions, including the effect of radiation pressure, are taken from Table 12 of Härm and Schwarzschild (Reference 19) with a change of scale as shown below.

Since $\kappa\epsilon_g$ is constant,

$$\frac{dP_g}{dP} = 1 - B \qquad \left(B = \frac{\kappa\epsilon_g}{4\pi cG}\right). \tag{37}$$

If we define

$$T = T_c\theta, \quad P_g = P_{g,c}\sigma, \quad M(r) = M_o\phi, \quad \text{and} \quad r = r_o\xi, \tag{38}$$

with

$$\left.\begin{aligned} M_o^2 &= \frac{3}{4\pi aG^3(1-B)^3}\,\frac{1-\beta_c}{\beta_c}\left(\frac{k}{\mu_c H}\right)^4, \\ r_o^2 &= \frac{1}{4\pi G(1-B)\beta_c P_c}\left(\frac{kT_c}{\mu_c H}\right)^2, \\ C^* &= \frac{B}{4(1-B)}\,\frac{\beta_c}{1-\beta_c}, \end{aligned}\right\} \tag{39}$$

the core equations are

$$\frac{d\sigma}{d\xi} = -\frac{\sigma\phi}{\xi^2\theta}, \quad \frac{d\phi}{d\xi} = \frac{\sigma\xi^2}{\theta}, \quad \text{and} \quad \frac{d\theta}{d\xi} = -C^*\frac{\sigma\phi}{\theta^4\xi^2}, \tag{40}$$

which are the equations solved by Sandage and Schwarzschild (Reference 18) for the case where radiation pressure is negligible.

The homology invariant functions defined by Equations 14 and 31 are given by

$$\left.\begin{aligned} U &= \frac{d\log\phi}{d\log\xi}; \\ V &= -\left(\frac{\beta}{1-B}\right)\frac{d\log\sigma}{d\log\xi}; \\ n+1 &= \left(\frac{\beta}{1-B}\right)\frac{d\log\sigma}{d\log\theta}. \end{aligned}\right\} \tag{41}$$

The reduction factor $\beta/(1-B)$ is expressed by using the integral of Equation 37 and the relation $P = P_{g,c}\sigma/\beta$, as

$$\frac{\beta}{1-B} = 1 - B - \frac{\beta_c \sigma}{\beta_c(1-\sigma)} . \tag{42}$$

Core solutions are specified by the values C* and β_c. For each value of C*, the fitting of U/μ and V/μ of the core and envelope solutions determines β_c and C, which in turn give L and L_g $\left(= Mq_1\epsilon_g\right)$. Then Equation 36 and $L_H = L - L_g$ determine T_1 and the other physical quantities. If these solutions are found for a sequence of stages, Equation 12 and then Equations 24 can be used to find the time interval and the estimate of hydrogen depletion, respectively:

$$t = \frac{3k}{2\mu_c H}\int \frac{T_c}{\epsilon_g} d\left[\ln T_c - \frac{2}{3}\ln\left(\frac{1-\beta_c}{\beta_c}\right) - \frac{8}{3}\left(\frac{1-\beta_c}{\beta_c}\right)\right] ; \tag{43}$$

$$\Delta \int X\, dq = -\frac{\int L_H\, dt}{ME_H} . \tag{44}$$

The results for Cases 1 and 2 are given in Table 2, and the evolutionary changes in the H-R, T_c-ρ_c, T_e-T_c, and color-magnitude (C-M) diagrams are illustrated in Figures 6, 7, 9, and 2, respectively. The difference between Cases 1 and 2 is found to be small, showing that results in this phase are not sensitive to the shape of the hydrogen distribution curve. The positions of the first stage, in the H-R diagram, are very near to those of the last stage of hydrogen exhaustion, but the central density is slightly higher. This is explained by the assumed uniformity of ϵ_g, since the central density required to sustain the core for a given value of L_g is lower if the energy source is more concentrated toward the center.

The contraction of the core stops when the central temperature becomes so high that the energy generation due to helium burning,

$$L_{3\alpha} = \epsilon^{o}_{3\alpha}\, Y^3 \left(\frac{3n_c' + 3}{3n_c' + s}\,\frac{k\rho_c T_c}{2G\mu_c H}\right)^{\frac{3}{2}} \left(\frac{T_c}{T_o}\right)^{s} , \tag{45}$$

where

$$n_c' = \frac{3(8 - 7\beta_c)}{8 - 3\beta_c - 3\beta_c^2} , \tag{45'}$$

becomes comparable with the gravitational energy, L_g. Equation 45 may be obtained from Equation 6 if we use a polytropic solution with index n_c' as an approximate solution for the

Table 2

Evolutionary Stages of Stars of M = 15.6 $M_\odot$ and M = 10.1 $M_\odot$

in the Gravitational Contraction Phase

$\left(\mu_e^2\, M/M_\odot = 4.468;\ X_{CNO} = 0.02/3\right)$

Parameter	Values in Stages 1 through 5†												
	M = 15.6 $M_\odot$ Case 1: $q_1 = 0.153$					M = 15.6 $M_\odot$ Case 2: $q_1 = 0.173$				M = 10.1 $M_\odot$ Case 1′: $q_1 = 0.189$			
	1	2	3	4	5	1	2	3	4	1	2	3	4
C*	0.2300	0.2132	0.2300	0.2459	0.2487	0.2300	0.2300	0.2459	0.2487	0.2300	0.2300	0.2459	0.2487
Log C	-2.979	-2.946	-2.913	-2.866	-2.806	-2.961	-2.930	-2.871	-2.827	-3.018	-2.909	-2.861	-2.814
$1 - \beta_c$	0.1471	0.0800	0.0527	0.0456	0.0455	0.1236	0.0814	0.0582	0.0568	0.1270	0.0307	0.0298	0.0305
Log T_c	7.745	7.805	7.919	8.153	8.331	7.780	7.852	8.088	8.247	7.715	7.928	8.156	8.332
Log ρ_c	1.611	2.089	2.626	3.393	3.928	1.803	2.222	3.086	3.575	1.595	2.897	3.594	4.111
Log $r_1/R_\odot$	-0.238	-0.315	-0.399	-0.549	-0.699	-0.245	-0.311	-0.460	-0.564				
Log T_1	7.584	7.626	7.663	7.721	7.771	7.584	7.614	7.662	7.692	7.566	7.665	7.720	7.769
Log ρ_1‡	0.976	1.040	1.081	1.161	1.215	0.905	0.937	0.965	0.984	1.020	1.124	1.202	1.268
Log U_1‡	0.211	0.044	-0.167	-0.533	-0.845	0.065	-0.099	-0.518	-0.813	0.239	-0.247	-0.599	-0.902
Log V_1‡	0.428	0.450	0.482	0.538	0.588	0.431	0.453	0.527	0.580	0.406	0.464	0.530	0.583
L_g/L	0.596	0.279	0.182	0.151	0.132	0.548	0.331	0.220	0.196	0.588	0.109	0.102	0.095
Log $R/R_\odot$	0.946	1.024	1.173	1.670	3.393	0.973	1.067	1.469	2.382	0.734	0.981	1.349	2.334
Log $L/L_\odot$	4.580	4.613	4.646	4.693	4.753	4.598	4.629	4.688	4.732	4.425	4.534	4.582	4.629
Log T_e	4.434	4.403	4.337	4.100	3.254	4.425	4.385	4.200	3.754	4.502	4.405	4.233	3.753
$t \times 10^{-5}$(yr.)	0.000	0.115	0.296	0.645	0.999	0.000	0.097	0.374	0.599				
$\Delta\int X\,dq \times 10^3$	0.000	-0.164	-0.564	-1.481	-2.566	0.000	-0.148	-0.771	-1.387				

†The onset of helium burning $\left(L_g = L_{3\alpha}\right)$ lies between Stages 4 and 5 of Case 1, and between Stages 3 and 4 of Cases 2 and 1′.

‡In Case 2 this refers to the external value.

central region. The onset of helium burning $\left(\text{when } L_g = L_{3\alpha}\right)$ is found to occur when

$$\log T_c = 8.21, \quad \log \rho_c = 3.46, \quad \log T_e = 3.92,$$

$$t = 0.68 \times 10^5 \text{ yr.}, \quad \text{and} \quad -\Delta\int X\,dq = 0.00148, \tag{46}$$

where t and $\Delta\int X\,dq$ are measured from the first stage of Case 1. This amount of hydrogen depletion corresponds to a change of q_1 from 0.153 to 0.180 in Equation 32. The values in Equations 46 themselves are computed from the results of Cases 1 and 2 by taking into account the effect of hydrogen depletion.

The dependence of the foregoing results on the age-zero chemical composition is shown by the results of similar computations performed for a star of age-zero composition,

$$X_e = 0.61, \quad Y_e = 0.37, \quad Z_e = 0.02, \quad \text{and} \quad X_{CNO} = 0.02/3 \quad \left(\mu_e = 0.663\right), \tag{47}$$

which seems to represent the young population I stars more closely than our adopted composition. Using, as before, $A = 16$ (Equations 19), i.e., maintaining $\mu_e^2 M/M_\odot = 4.468$, we find the corresponding mass to be $M = 10.1\ M_\odot$. As long as the opacity is due to electron scattering alone and the shell source energy is negligible, the solutions for the hydrogen burning phase (Reference 1) are invariant for the homology transformations which keep the value for $\mu_e^2 M$ and $L\left(1 + X_e\right)/M$ in Equations 19 constant. The explanation for this is that the basic equations depend on the composition only through l and j, and these are related approximately by $j = l^{0.285}$, so that l and j themselves are invariant functions of q for the above transformation. The invariance of l gives as a relation between the old and new hydrogen contents, $X(q)$ and $X'(q)$, respectively:

$$\frac{1.496}{X(q) + 0.596} = \frac{1.206}{X'(q) + 0.596}. \tag{48}$$

In the region where X' is small,

$$X'(q) = 3.96(q - 0.189). \tag{49}$$

The results of the computations with the new composition and with $q_1 = 0.189$ are given in Table 2 (Case 1') and illustrated in Figures 6 and 7. The onset of helium burning occurs at the point where

$$\log T_c = 8.19 \quad \text{and} \quad \log T_e = 4.18 \tag{50}$$

(cf. Equations 46). Figure 6 indicates that the point in the H-R diagram corresponding to the onset of helium burning is more sensitive to the age-zero composition than are the points for the hydrogen burning phase.

If 0.02 is used instead of 0.02/3 as the value for X_{CNO}, the solutions in Table 2 vary as follows: Log T_1 and log T_c decrease by an amount 0.028, as derived from Equation 36, since L_H and L_g do not change; log $R/R_\odot$ increases by the same amount; and log T_e decreases by 0.014. This relative change in log T_e, which is due to the difference in composition, is more reliable than the values themselves in view of the inevitable uncertainties which are due to adopted assumptions. Figure 9 shows that a higher abundance of the CNO group leads to a lower surface temperature, and that a higher helium content leads to a higher surface temperature.

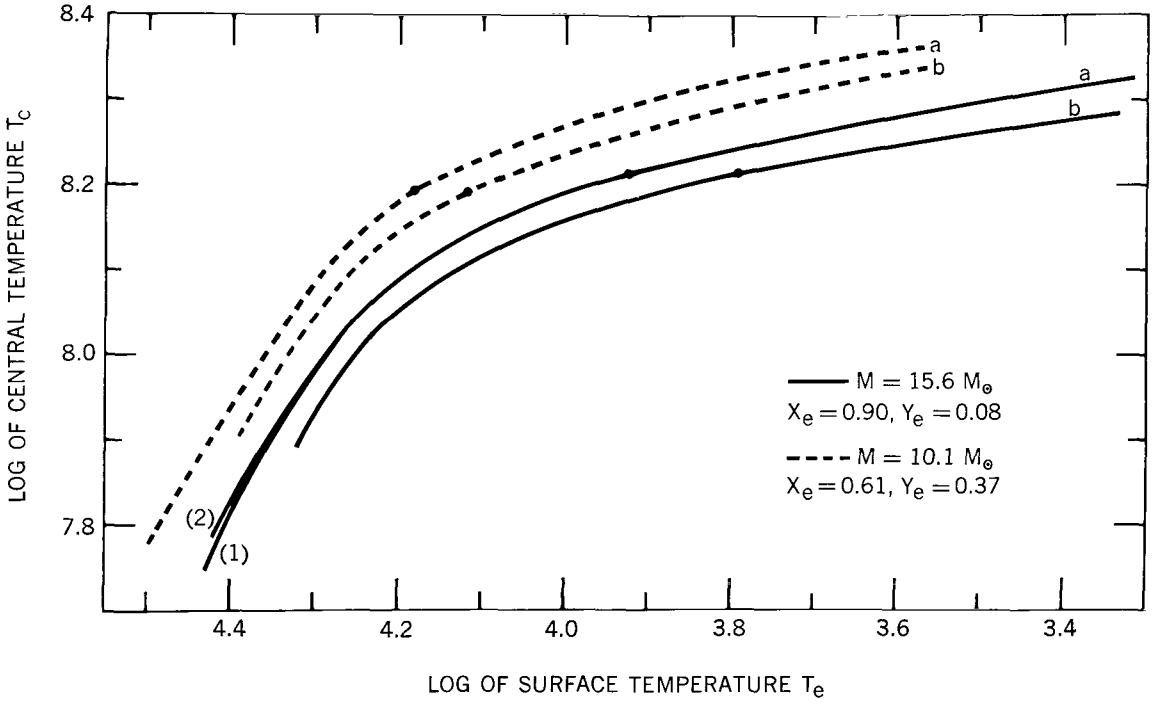

Figure 9 — Variation of surface temperature with central temperature in the gravitational contraction phase. Curves marked *a* are for stars with $X_{CNO} = 0.02/3$; curves *b* for $X_{CNO} = 0.02$. Branches (1) and (2) of the solid *a* curve show the small difference between Cases 1 and 2 (Table 2), respectively. Table 2 also gives the data for the dashed *a* curve. The points on the curves correspond to the onset of helium burning $(L_g = L_{3\alpha})$.

THE HELIUM BURNING PHASE

After helium burning begins, the gravitational energy released becomes negligible and a convective core appears in the central region. The early stages of this phase were computed in Reference 2 under the simplifying assumption of constant mean molecular weight in the core. We will now reconsider and extend these computations up to the point where helium is almost completely consumed, taking into account the change of mean molecular weight which is due to the conversion of helium into carbon, and also the change of rate of helium burning which is due to a changing central temperature. Computations for this phase were actually completed prior to those of the previous phases.

The stellar interior now consists of three regions (Figure 1): (1) a radiative envelope outside the hydrogen burning shell, which retains the composition

$$\left.\begin{aligned} X &= 0.90 && (q \geq 0.415)\ , \\ &= 3.25\, q - 0.4488 && (0.415 \geq q > q_1)\ ; \end{aligned}\right\} \qquad (51)$$

(2) a radiative zone with uniform composition and constant $L(r)$ between the shell and the convective core,

$$X = 0, \quad Y = 0.98, \quad \text{and} \quad L(r) = L_{3\alpha} \qquad (q_1 > q > q_f)\ ; \qquad (52)$$

and (3) a convective core with uniform composition,

$$X = 0, \quad Y = Y_c, \quad \text{and} \quad Z = 1 - Y_c \qquad (q_f > q \geq 0)\ . \qquad (53)$$

The adopted expression for $X(q)$ in Equation 51 differs only very slightly from that in Equation 23, which, strictly speaking, would be preferred. The hydrogen content is assumed to change abruptly at the point q_1. This point will be discussed at the end of this section.

The mass of the convective core, q_f, was found to increase monotonically (at least until Y_c has decreased to a value as small as 0.016). A retreating core (as in hydrogen burning) leaves an inhomogeneous radiative zone behind, whose composition as a function of q depends upon its evolutionary history; an advancing core does not introduce this complication.

The envelope solutions were integrated with three input parameters, C, q_1, and $L_{3\alpha}/L$, from the surface to the point where convective instability sets in, i.e., where $(n+1)_{rad}$ and $(n+1)_{conv}$, as defined in Equations 15, become equal.

Solutions for the convective core are specified by one parameter, β_c. For each stage, with its given set of values of q_1 and Y_c, fitting of the envelope and core solutions was accomplished by imposing the condition of continuity of U/μ, V/μ, and β at q_1, to give a family of mathematical solutions specified by a single parameter C. Then the formulas for $L_{3\alpha}$ (Equation 45) and

$$L_H = \epsilon_H^o X_{1e} X_{CNO} \rho_{1e}^2 \left(\frac{T_1}{T_o}\right)^s \frac{4\pi r_1^3}{V_{1e}\left[2 + \frac{s-2}{(n+1)_{1e}}\right] - 3} \tag{54}$$

determine the solution completely. The letter e in the subscript indicates the external side of the interface at the edge of the convective core.

For the first stage we assumed $q_1 = 0.195$ and $Y_c = 0.98$. This value of q_1 is not much different from the value 0.180 found for the onset of helium burning $(L_g = L_{3\alpha})$ in the gravitational contraction phase. Moreover, the depletion of hydrogen was found to be much faster than that of helium in the early stages of helium burning, so that no significant error is introduced by the adoption of these initial values for q_1 and Y_c. We chose a series of values of q_1, in order to produce a time sequence of stages, and estimated the corresponding value of Y_c in computing the first iteration for each stage. A corrected value of Y_c could then be computed from

$$\frac{E_{3\alpha}}{L_{3\alpha}} \Delta \int Y\, dq = \frac{E_H}{L_H} \Delta \int X\, dq = -\frac{\Delta t}{M} , \tag{55}$$

where $E_{3\alpha} = 5.8 \times 10^{17}$ ergs/gm is the energy released by the conversion of one gram of helium into carbon. In practice, it was found that two iterations were sufficient before proceeding to the next stage. The results are summarized in Table 3, the last three rows of which give the constants used in the expressions for $\epsilon_{3\alpha}$ and $L_{3\alpha}$ in Equations 6 and 45, respectively. Figure 6 shows the evolutionary track in the H-R diagram; Figure 7, the T_c-ρ_c curve; Figures 8 and 10, the distribution of the chemical composition; and Figure 2, the track in the C-M diagram. Parenthetically, we note the empirical result that $L_{3\alpha}$ and L_H are extremely linear as functions of Y_c throughout Stages 1-5 of Table 3.

In the early stages, when $L_{3\alpha}/L$ and q_1 increase with time but Y_c does not change appreciably, the core expands while the star contracts as a whole. As Y_c becomes sufficiently small, T_c increases more rapidly than T_1, thus keeping $L_{3\alpha}$ nearly constant, since it is proportional to Y_c^3. The presently used stellar model, with two energy sources, is sensitive to the value of T_c/T_1 in such a way that an increase in this ratio gives rise to contraction of the core and rapid expansion of the envelope.

Table 3

Evolutionary Stages of a Star of $M = 15.6\ M_\odot$ in the Helium Burning Phase*

$(\mu_e^2\, M/M_\odot = 4.468)$†

Parameter	Values in Stages 1 through 7						
	1	2	3	4	5	6	7
Log C	-2.826	-2.813	-2.804	-2.797	-2.786	-2.761	-2.736
$t \times 10^{-5}$ (yr.)	0.000	3.204	5.901	8.167	10.155	11.340	11.543
$1 - \beta_c$	0.105	0.146	0.176	0.203	0.228	0.244	0.246
Log T_c	8.219	8.247	8.273	8.302	8.350	8.442	8.501
Log ρ_c	3.201	3.146	3.152	3.189	3.294	3.548	3.723
Log P_c	19.257	19.226	19.248	19.303	19.444	19.781	20.014
$Y_c = Y_{fi}$	0.980	0.762	0.552	0.353	0.162	0.0392	0.0164
$\mu_c = \mu_{fi}$	1.340	1.419	1.504	1.594	1.692	1.763	1.776
q_f	0.080	0.107	0.126	0.141	0.153	0.160	0.161
Log r_f/R	-2.884	-2.592	-2.472	-2.432	-2.509	-3.004	-3.744
Log U_{fe}	0.310	0.254	0.201	0.150	0.096	0.058	0.050
Log V_{fe}	0.490	0.490	0.512	0.525	0.536	0.544	0.546
$(n+1)_f$	2.906	3.035	3.123	3.182	3.257	3.292	3.296
$1 - \beta_f$	0.066	0.093	0.114	0.130	0.151	0.162	0.164
Log T_f	8.016	8.021	8.027	8.025	8.067	8.144	8.199
Log ρ_{fe}	2.814	2.664	2.584	2.514	2.562	2.756	2.919
Log P_f	18.648	18.517	18.453	18.388	18.490	18.766	18.985
q_1	0.195	0.232	0.252	0.265	0.274	0.279	0.280
Log r_1/R	-2.498	-2.235	-2.128	-2.091	-2.161	-2.630	-3.353
Log U_{1e}	-0.848	-0.873	-0.897	-0.920	-0.976	-1.127	-1.244
Log V_{1e}	0.555	0.548	0.544	0.542	0.549	0.574	0.589
$(n+1)_{1e}$	3.927	3.934	3.939	3.942	3.951	3.970	3.978
$1 - \beta_1$	0.300	0.286	0.283	0.283	0.287	0.303	0.321
Log T_1	7.674	7.657	7.650	7.645	7.644	7.656	7.668
Log ρ_{1e}	0.887	0.802	0.756	0.723	0.699	0.693	0.693
Log P_1	16.622	16.574	16.549	16.530	16.520	16.543	16.567
X_{1e}	0.185	0.305	0.371	0.413	0.443	0.459	0.462
μ_{1e}	1.024	0.887	0.826	0.792	0.769	0.758	0.756
$L_{3\alpha}/L$	0.145	0.254	0.351	0.437	0.516	0.541	0.518
Log $L_{3\alpha}/L_\odot$	3.882	4.140	4.288	4.391	4.475	4.520	4.526
Log $L_H/L_\odot$	4.654	4.607	4.556	4.502	4.447	4.449	4.494
Log $L/L_\odot$	4.722	4.735	4.744	4.751	4.762	4.787	4.812
Log $R/R_\odot$	1.971	1.754	1.666	1.640	1.704	2.127	2.812
Log T_e	3.959	4.070	4.117	4.132	4.102	3.897	3.561
M_{bol}	-7.201	-7.233	-7.255	-7.274	-7.302	-7.364	-7.425
M_v	-6.82	-6.38	-6.16	-6.09	-6.29	-7.20	-6.23
B - V	0.09	-0.05	-0.10	-0.14	-0.09	0.08	1.34
Log $\epsilon_{3\alpha}^\circ$	-1.886	-0.049	-0.049	0.856	1.745	2.897	3.761
$s_{3\alpha}$	25.80	21.00	21.00	18.60	16.20	13.00	10.50
$T_{o,3\alpha} \times 10^{-8}$ (°K)	1.500	1.800	1.800	2.000	2.250	2.700	3.200

*In this phase we have adopted log $L_\odot = 33.5932$, corresponding to a value of the solar constant, $Q = 2$ gm-cal/cm^2-min (see the section entitled "Definitions and Basic Equations," page 5).

†Additional constant quantities: $Y_{fe} = Y_{1i} = 0.98$; $\mu_{fe} = \mu_{1i} = 1.340$; $q_b = 0.415$; and $\mu_e = 0.535$. The letters i and e following 1, 2, or f in a subscript indicate the internal or external side of the interface. The subscript b is used to designate the lower boundary of the radiative zone with initial composition.

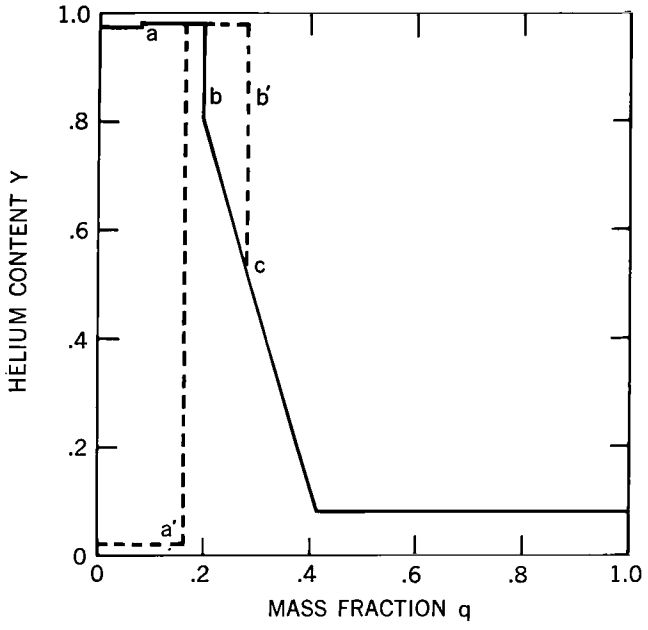

Figure 10—Distribution of the helium content Y during helium burning (cf. Figure 8), for a point in time just after Stage 1 of Table 3 (solid lines), and for Stage 7 (dashed lines). From point c toward higher q-values the curves are common. The points a and a' indicate the q-values for the boundary of the convective core; the segments b and b', the q-values of the hydrogen burning shell.

Let us consider the point in the H-R diagram corresponding to Stage 1 of helium burning. Reference 2 shows that, for the composition of Equations 47, with $M = 10.1\ M_\odot$ this point is shifted horizontally by an amount $\Delta \log T_e \approx 0.3$; for the standard composition (Equation 1) at 1/10 of Salpeter's 3α-reaction rate, the shift in $\Delta \log T_e \approx -0.3$. Since it was shown in Reference 2 that it is the ratio $\epsilon_H / \epsilon_{3\alpha}$ that is important in the present consideration, it follows that a shift to the right in the H-R diagram will also result from an increase in the abundance of the CNO group. The tendencies deduced in regard to changes of the basic quantities of the gravitational contraction phase thus are also true for the helium burning phase.

In the computations for the helium burning phase, the hydrogen burning shell is assumed to be infinitely thin and there is assumed to be a discontinuity in X at the point q_1. Computations taking into account the finite width of the shell, in which $X(q)$ and $L(r)$ vary continuously, will not be simple since $X(q)$ depends upon the evolutionary history. An approximate computation for a finite shell has already been made by using the solution for the first stage as a first approximation, with the shell defined as the region where $L_c \leq L(r) \leq 0.9\ L$, and under the assumption that

$$\frac{X}{X_o} = \frac{L(r) - L_c}{0.9L - L_c}, \tag{56}$$

where X_o is the hydrogen content at the outer edge of the shell. The result shows that the mass fraction in the shell is $\Delta q = 0.025$, and that the correction to the first approximation is about 0.03 for $\log T_e$.

The energy generation expression (Equation 6) corresponds to the reaction $3\alpha \rightarrow C^{12}$. As the concentration of carbon increases, the reactions $C^{12}(\alpha,\gamma)O^{16}$ and $O^{16}(\alpha,\gamma)Ne^{20}$ become appreciable.* Since the ranges of the central temperature and density are known from Table 3, the change of the relative abundances of helium, carbon, oxygen, and neon can be computed as indicated by Hayakawa, et al. (Reference 20). The total energy generation and the rate of consumption of helium are expressed approximately by

$$\epsilon = \epsilon_{3\alpha} \left(1 + 0.1\, Y^{-2}\right) , \tag{57}$$

and

$$\frac{d\left(\int Y\, dq\right)}{dt} = \frac{\int \epsilon\, dq}{E_{3\alpha}} \left(\frac{Y^2 + 0.04}{Y^2 + 0.1}\right) . \tag{58}$$

The final abundance X_c of carbon, when helium has been exhausted, is approximately 0.1.

The numerical values in the preceding paragraph have an uncertainty factor of 3, because of a large uncertainty in the reaction rates of $C^{12}(\alpha,\gamma)O^{16}$ and $O^{16}(\alpha,\gamma)Ne^{20}$. The adoption of Equations 57 and 58 changes the results of Stages 6 and 7 in Table 3 in such a way that T_c becomes somewhat lower and T_e higher, for the same values of Y_c.

THE CARBON AND NEON BURNING PHASES

As helium is further consumed in the central region, the convective core continues to retreat. After the complete exhaustion of helium, the inner regions begin to contract, helium burning begins in an outer shell, and the central temperature increases until the onset of carbon or neon burning. The time scale of this gravitational contraction of the core is so short that the depletion of hydrogen and helium in their respective shells is very small. Carbon burning follows gravitational contraction if the products of helium burning include an appreciable amount of C^{12}. If, however, the final products are mainly neon and oxygen, neon burning takes place. Since there is, at the present time, some uncertainty in the relative abundances of these final products, and it is known that phases of both carbon and neon burning occur, the two extreme cases will be considered here: pure carbon burning $(Z_{core} = X_C = 1)$; and pure neon burning $(Z_{core} = X_{Ne} = 1)$. In each case the initial q-values corresponding to the helium and hydrogen burning shells are taken as identical with the q-values for the hydrogen shell and the convective core boundary, respectively, of Stage 7 of the helium burning phase. These values are $q_1 = 0.280$ and $q_2 = 0.162$. The envelope, which is taken to be the region exterior to q_2, has the same composition here as in Stage 7 of helium burning. The envelope solution is specified by the parameters C and L_H/L. The core then consists of the central convective region $(q_f \geq q \geq 0)$ and the outer radiative

*But see the remarks at the end of the next section, "The Carbon and Neon Burning Phases."

Table 4
Structure of a Star of $M = 15.6\ M_\odot$ at the Onsets of the Carbon and Neon Burning Phases
$(\mu_e^2\ M/M_\odot = 4.468)$

Parameter	Carbon Burning $X_C = 1$	Neon Burning $X_{Ne} = 1$
Log C	-2.63	-2.50
Log $L/L_\odot$	4.95	5.07
Log $R/R_\odot$	10.0	26.7
$1 - \beta_c$	0.21	0.18
Log T_c	8.83	9.04
Log ρ_c	4.63	4.57
$1 - \beta_2$	0.46	0.58
Log T_2	8.30	8.36
Log ρ_{2e}	2.57	2.57
$1 - \beta_1$	0.42	0.55
Log T_1	7.07	6.70
Log ρ_{1e}	-1.3	-2.6
L_{core}/L	0.19	0.12
$L_{3\alpha}/L$	0.81	0.88
L_H/L	0.00	0.00
q_f	0.105	0.114
Log U_f	0.25	0.17
Log V_f	0.56	0.69
$1 - \beta_f$	0.12	0.15
q_2	0.161*	0.161*
Log U_{2e}	-0.85	-1.28
Log V_{2e}	0.45	0.43
q_1	0.280*	0.280*
Log U_{1e}	-1.63	-2.01
Log V_{1e}	0.60	0.60

*Taken from the last stage of Table 3 (helium burning).

zone $(q_2 > q \geq q_f)$, both of which are devoid of hydrogen and helium. Two parameters specify the core solutions: L_{core}, the energy production due to carbon or neon burning in the central region, and β_c.

The two solutions are fitted at q_2 by imposing the condition of continuity of U/μ and V/μ. The energy generation equations for L_{core} and $L_{3\alpha}$ are expressed in forms similar to those of Equation 45 and 54, respectively, but with some changes because of the different dependence of ϵ on the density (Appendix A). The three energy-generation equations for $L_{3\alpha}(L - L_H - L_{core})$, L_{core}, and L_H, together with the condition of the continuity of U/μ and V/μ, determine the four parameters of the envelope and core solutions and fix the scale of the radius. The results are shown in Table 4. The values at the onset of carbon burning in the T_c-ρ_c diagram are pictured in Figure 4.

For both carbon and neon burning the envelope is so tremendously extensive and the temperature in the hydrogen burning shell so low, energy production in the shell is negligible. The huge stellar radius indicates the necessity (as anticipated) for introducing a surface convection zone. When this region is taken into account the radius becomes considerably less;† but the inner structure should remain essentially the same,† according to the inference to be drawn from the work of Hoyle and Schwarzschild (Reference 6) on the red-gaint branch of the globular clusters. It seems very probable that massive red supergiants are in the carbon and neon burning or later phases of their evolutionary history.†

†This expectation has been confirmed by recent computations, the results of which will be published later.

EVOLUTION BEYOND CARBON AND NEON BURNING

After the completion of carbon and neon burning, heavier nuclei will be built up successively by heavy-ion reactions, such as $O^{16} + O^{16}$, and by the capturing reactions of alpha particles, protons, and neutrons, which are produced by photodissociation. The build-up processes continue in the central region until the iron group is formed and the nuclear energy exhausted.

The lifetime of the star in carbon and neon burning and later phases is estimated as follows: According to the results of previous sections, the mass fraction of the iron core is, approximately, $q = 0.15$, and the energy generation, $L_{core}/L = 1/3$. The energy release per gram of matter, E, which is due to the conversion of carbon into iron, is 10.3×10^{17} ergs/gm, of which 5.6×10^{17} ergs/gm are liberated in carbon burning; that which is due to the conversion of neon into iron is 6.9×10^{17} ergs/gm, of which about 1.1×10^{17} ergs/gm are liberated in neon burning. If we take $E = 10^{18}$ ergs/gm and $L = 10^5\ L_\odot$, the stellar lifetime of a red supergiant is

$$t = \frac{EMq}{L} \frac{L}{L_{core}} = 12 \times 10^5 \text{ yr.} \quad , \tag{59}$$

with an uncertainty factor of 3 at most.

If we adopt the rate of mass ejection $dM/dt = -4 \times 10^{-6}\ M_\odot$/yr. derived for α Orionis ($M \approx 20\,M_\odot$) by Weymann (Reference 21), the mass fraction lost during 1.2×10^6 years is about 20 percent; however there is a large uncertainty factor in the ejection rate at the present time.

Gove, et al. (Reference 22) found the spin and parity of the 4.97-Mev level of Ne^{20} to be 2^-; this means that the reaction $O^{16}(\alpha,\gamma)\ Ne^{20}$ in the helium burning phase may be neglected.* Eventually, neon will be formed as a product of C-C reaction and neon burning will take place after the carbon has been exhausted.

The papers of Chiu and Morrison (Reference 23), Chiu and Stabler (Reference 24), and Chiu (Reference 25) also contain information about the later evolutionary phases. These reports evaluate the rate of energy loss, by neutrino emission, from annihilation of electron-positron pairs (which are present at high temperature) and from the photo-neutrino effect, assuming the universal Fermi interaction between electrons and neutrinos. Their results show that the energy loss by neutrino emission may not be neglected in the carbon and neon burning and later evolutionary phases, if the above assumption on the universal Fermi interaction holds. Neutrino effects will be considered in a future paper.

*This result supersedes an earlier assignment, 2^+.

DISCUSSION

U-V Diagram

The characteristic change of the stellar structure due to the exhaustion of successively heavier nuclear fuels in the center can easily be seen in the U-V diagram shown in Figure 11. As the inhomogeneity of the chemical composition increases, the U-V curve moves more and more to the left, except for the innermost region (log V< approx. 0.3). The shift is particularly large in the region which forms a loop, that is, in the neighborhood of the shell energy sources, where the changes in the energy flux and the mean molecular weight are considerable. A large shift corresponds to a large change in the stellar radius for a given central temperature.

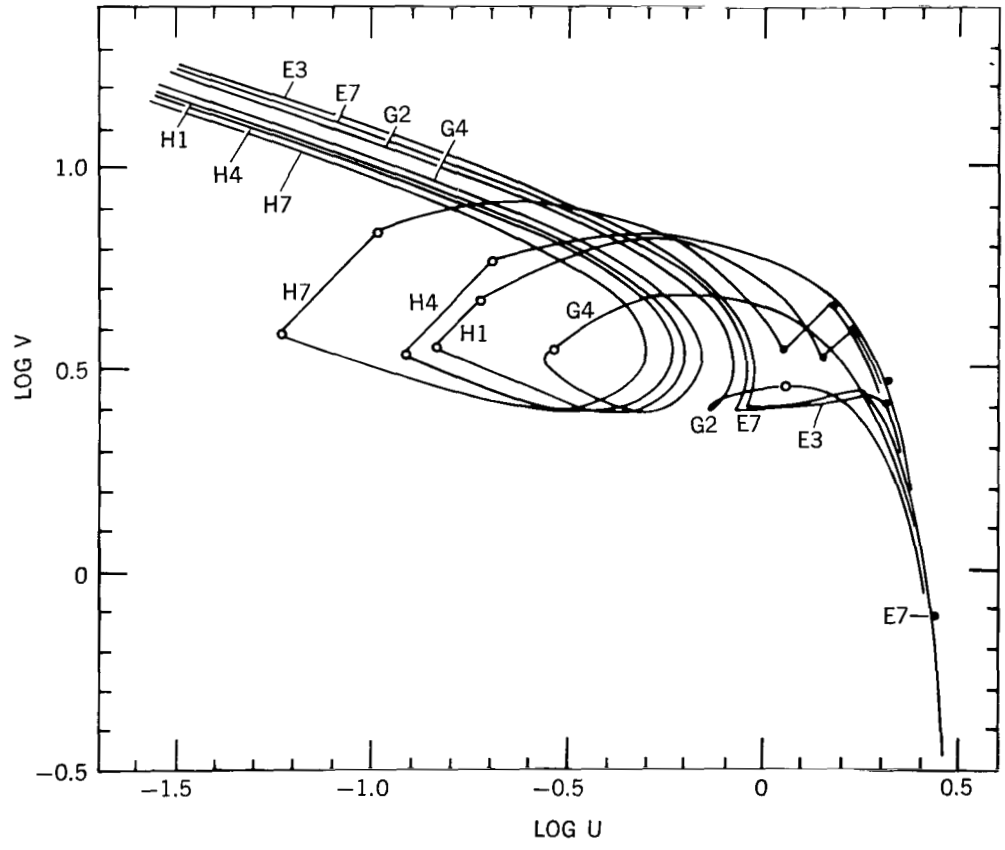

Figure 11 — The U-V curves for a star of mass $M = 15.6 M_{\odot}$ and $\mu_e = 0.535$. Letters on the curves refer to evolutionary phases as follows: E, hydrogen exhaustion (Table 1); G, gravitational contraction (Table 2); and H, helium burning (Table 3). Numbers refer to stages listed in these tables. Open circles indicate points corresponding to the hydrogen burning shells; closed circles, points corresponding to the boundaries of the convective cores.

Lifetime of a Massive Star

The time a star of mass $M = 15.6\ M_\odot$ and $\mu_e = 0.535$ spends in each of its evolutionary phases, from pre-main-sequence contraction to iron-core formation, is given in Table 5. The star spends approximately 98 percent of its helium burning lifetime in the early supergiant branch, before crossing the Hertzsprung gap. It is expected that the M-type supergiant branch consists of stars in the carbon and neon burning and later evolutionary phases.

Table 5
Time a Star of Mass $M = 15.6\ M_\odot$ Spends in Successive Evolutionary Phases $\left(\mu_e^2\ M/M_\odot = 4.468\right)$

Evolutionary Phase	Time (10^5 yr)
Pre-main-sequence contraction	~1
Hydrogen burning	156*
Hydrogen exhaustion	1.4
Gravitational (core) contraction	0.7
Helium burning	11.6
Gravitational (core) contraction	~0.5
Carbon and neon burning and later phases†	~12
Total	183

*Corrected value based on the computations of Reference 1.
†Through iron-core formation.

Comparison of Results with Observation

Some preliminary comparisons have been made between the theoretical results and observations of the double cluster h and χ Persei (NGC 869 and NGC 884). Although the conclusions from these comparisons cannot be regarded as definitive in view of various uncertainties and the limited useful data at hand, it appears that the theoretical results are in agreement with the observations. Before we give the details, however, a brief description of h and χ Persei is in order.

The cluster centers (which are separated by about 25' of arc) are located approximately in the galactic coordinates, $l = 103$ degrees, $b = -3$ degrees at a distance of 2.3 kiloparsecs (the true distance modulus is $m_o - M = 11.8$ mag., where m_o is the apparent magnitude corrected for absorption, and M is the absolute magnitude). The mean visual apparent distance modulus is, roughly, $m - M = 13.5$ mag.; it is well known however that the absorption is extremely patchy. The star densities in the two clusters are comparable.

According to a study by Artyukhina and Kholopov (Reference 26), although the densities are very high in the nuclear regions of these clusters, they fall off rapidly at angular distances greater than about 10' from the centers. The cluster nuclei are surrounded by

an extensive halo or association. Sharpless (Reference 27) established the membership of M-type supergiants as distant as 7° of arc. There is evidence of asymmetry of distribution and of local condensation in both the halo and the nuclei.

The computed evolutionary track of a star of 15.6 solar masses is compared, in Figure 2, with the C-M diagram of some of the brightest stars of h and χ Persei, based on the observations of Johnson and Morgan (Reference 28). The early main-sequence stars were reduced by means of the nomogram of Johnson (Reference 29, Figure 4) and the early supergiants were reduced by adopting the mean intrinsic colors of Johnson's Table III. The theoretical values of T_e and M_{bol} were converted to B - V and M_v by means of Table 1 in Reference 30, by taking B - V and the bolometric correction to be functions of T_e. Stars plotted in Figure 2 represent, in general, only a sampling; however, certain regions of this diagram are known to be essentially complete: the early and late supergiant branches of the nuclei (including stars within 23' of arc of either nucleus) and the late supergiant branch of the outer association (including stars out to an angular distance of 4°0), except for three M-type supergiant cluster members identified by Sharpless (Reference 27) which were not plotted because of imprecise data on absorption.

In the C-M diagram of h and χ Persei there is some indication of a gap, in both coordinates, between the uppermost main-sequence stars (burning hydrogen) and the stars of the early supergiant branch (burning helium), as the theoretical evolutionary track would lead us to expect. The gap is shown quite clearly in the C-M diagrams of the so-called "blue globular clusters",* NGC 330 and NGC 458, in the Small Magellanic Cloud (References 11 and 12).

For a group of stars born at the same time it is clear that little scatter is expected to appear in the magnitudes of the stars populating the supergiant branch. Furthermore it is suspected that in h and χ Persei the stars of the highly condensed nuclei most nearly fulfill this condition. As we consider stars of greater angular distance we encounter the possibility of multiple condensations with, perhaps, initial mass distributions which are not identical. In such a case we would expect a greater dispersion in the magnitudes of the stars of the early supergiant branch and a smaller separation of these stars from the upper main sequence. A comparison of the C-M diagrams of nuclear and outer stars (see Figure 2) gives some indication of such an effect.

The observed relative numbers of stars in h and χ Persei in the three regions, upper main sequence, early supergiant branch, and late supergiant branch, are not inconsistent with the corresponding times given in Table 5. Since the observational data of Figure 2 are largely incomplete, Table 6—based primarily on the data of Oosterhoff (Reference 31)—giving the separate luminosity functions of h and χ Persei for stars within 10' of arc of the

*The kinship of these objects with the open clusters rather than the globular clusters of our galaxy has been established. In fact NGC 330 resembles h and Persei closely in regard to the true diameter of the cluster and the absolute magnitude of the early supergiants and the brightest main-sequence stars (Reference 12).

cluster centers, was prepared. For both clusters the procedure followed in this paper is the same as that adopted by Sandage (Reference 32), in his determination of the luminosity function of h Persi, except for two minor differences: (1) we used our reductions of the UBV observations of Johnson and Morgan when available (12 stars), instead of using mean absorption; and (2) we used Oosterhoff's geometrical center for h Persei (star number 922) instead of BD + 56°522, originally adopted by van Maanen (Reference 33). The center adopted for χ Persei was star number 2235 (Reference 31). Cluster nonmembers were rejected on the basis of van Maanen's proper-motion studies in the case of h Persei; and on the basis of color, for five low-luminosity stars in the region of χ Persei.

Table 6
Observed Luminosity Functions for h and χ Persei
(Limiting Radius: 10' of Arc from Respective Centers)

Absolute Visual Magnitude	Observed Numbers	
	h Persei	χ Persei
-7.50 to -7.01	2*	1*
-7.00 to -6.51	0	1*
-6.50 to -6.01	0	0
-6.00 to -5.51	0	0
-5.50 to -5.01	1	3†
-5.00 to -4.51	2	2
-4.50 to -4.01	8	11
-4.00 to -3.51	9	5
-3.50 to -3.01	6	1
-3.00 to -2.51	15	11

*Stars in the helium burning phase.

†Includes two M-type supergiants (carbon and neon burning or later phases).

Let us assume that the stars of h and χ Persei were born at the same time. Consider an upper main-sequence star of mass $\mathfrak{M}_0$ whose mean luminosity during its hydrogen burning lifetime, $t_{H,0}$, is $< L_0 >$ corresponding to magnitude $< M_{v,0} >$. Now assume that for all upper main-sequence stars, $t_H \sim \mathfrak{M} / < L >$, $< L > \sim \mathfrak{M}^3$, and, for simplicity, that the helium burning lifetime is constant at 11.6×10^5 years.

A simple computation shows that a slightly more massive star of magnitude $< M_{v,1} > = < M_{v,0} > - \Delta M$, where $\Delta M = 0.4343 \times 1.5 \times 2.5 \times 11.6/156 = 0.12$ magnitude, will have completed both hydrogen and helium burning during the time interval $t_{H,0}$.

The conclusion to be drawn from the foregoing computation is that the number of stars per 0.12 magnitude at the "knee" (absolute visual magnitude, $M_v \geq -4.50$, Table 6) of the upper main-sequence luminosity function should be approximately equal to the observed number of supergiants in the helium burning phase.* The "knee" occurs where expected

*Note that although some of the early-type stars in the range $-5.50 \leq M_v \leq -4.01$ are known to be in luminosity class I, the C-M diagram shows that these stars are still in the hydrogen burning phase.

on the basis of computations for a star of $\mathfrak{M} = 15.6\ \mathfrak{M}_\odot$, i.e., about 3 magnitudes fainter than the helium burning supergiants.

By considering the dispersion in magnitude of the helium burning stars, we can determine the required density of stars over a range of one magnitude at the "knee." The results are 1.9 stars in h Persei and 2.0 stars in χ Persei per 0.12 magnitude. If slightly more or less smoothing of the luminosity function is performed in the computation, the result is nearly the same, viz., a prediction of two helium burning supergiants for each cluster, which corresponds with observations.

Since M-type supergiants are expected to be in phases from carbon and neon burning to iron-core formation (supernova explosion), Table 5 shows that roughly equal numbers of stars should populate the early and late supergiant branches of clusters, where the stars considered have masses of about 15 $M_\odot$ and ages > about 15 million years. In view of all the uncertainties involved, Table 7 would indicate that the ratio is really not markedly different from 1:1.

Table 7
Approximate Numbers of Stars in the Supergiant Branches of h and χ Persei and NGC 330

Cluster	Early Supergiants	Late Supergiants
h and χ Persei:		
(r < 10')*	4	2
(r < 23')†	6	6
(r < 1°.0)	9‡	9
(r < 1°.5)	14‡	11
(r < 2°.0)	19‡	12
(r < 2°.5)	19‡	13§
NGC 330‖	10	15

* Data from Table 6.

† Data from Figure 2.

‡ *Minimum numbers, but fairly complete, especially for the lower limiting radii.* Counts given are numbers of stars (to be found in the "Henry Draper Catalog") observed by Johnson and Morgan (Reference 28, Table 2) and Johnson and Hiltner (Reference 34, Table 7).

§ Minimum number. The maximum number is 18, based on the results of the Case Institute surveys (see literature cited by Sharpless in Reference 27).

‖ Data from the C-M diagram by Arp (Reference 12). He states that almost all of the stars observed by him are cluster members and that the observations are essentially complete.

Comparison with the Evolution of Less Massive Stars

There is an essential difference between the massive stars studied here and less massive stars, in regard to the evolutionary stage at which electron degeneracy sets in. Figure 7 shows that in the massive stars there is an approximate proportionality between ρ_c and T_c^3, and that electron degeneracy does not appear, at least up to the carbon burning stage. On the contrary, for stars of M < about 4 $M_\odot$, electron degeneracy is expected to begin in the hydrogen exhaustion or core contraction phase, before the onset of helium burning. The red giant branch of galactic clusters less luminous than M41 are burning hydrogen in a shell, as in the case of M67 (Reference 4); but the red supergiant branches of

h and χ Persei and NGC 330, for example, will be explained by evolutionary phases more advanced than helium burning.

ACKNOWLEDGMENTS

The authors are grateful to Drs. R. Jastrow and J. A. O'Keefe for their encouragement, and to Mr. W. F. Cahill and Mr. D. Sumida for the programming and arrangement of the IBM 704 and 7090 computations.

REFERENCES

1. Sakashita, S., Ono, Y., and Hayashi, C., "The Evolution of Massive Stars. I," *Prog. Theoret. Phys.* 21(2):315-323, February 1959

2. Hayashi, C., Jugaku, J., and Nishida, M., "Evolution of Massive Stars. II. Helium-Burning Stage," *Prog. Theoret. Phys.* 22(4):531-543, October 1959

3. Burbidge, E. M., Burbidge, G. R., Fowler, W. A., and Hoyle, F., "Synthesis of the Elements in Stars," *Rev. Modern Phys.* 29(4):547-650, October 1957

4. Hoyle, F., and Schwarzschild, M., "On the Evolution of Type II Stars," *Astrophys. J. Suppl. Ser.* 2(13):1-40, June 1955

5. Tayler, R. J., "Evolution of Massive Stars," *Astrophys. J.* 120(2):332-341, September 1954

6. Kushwaha, R. S., "The Evolution of Early Main-Sequence Stars," *Astrophys. J.* 125(1):242-259, January 1957

7. Blackler, J. M., "Models for Main Sequence Stars," *Mon. Not. Roy. Astronom. Soc.* 118(1):37-44, 1958

8. Schwarzschild, M., and Härm, R., "Evolution of Very Massive Stars," *Astrophys. J.* 128(2):348-360, September 1958

9. Henyey, L. G., LeLevier, R., and Levee, R. D., "Evolution of Main-Sequence Stars," *Astronom. J.* 129(1):2-19, January 1959

10. Hoyle, F., "On the Main-Sequence Band and the Hertzsprung Gap," *Mon. Not. Roy. Astronom. Soc.* 120(1):22-32, 1960

11. Arp, H., "Southern Hemisphere Photometry VI; The Color-Magnitude Diagram of NGC 458 and the Adjoining Region of the Small Magellanic Cloud," *Astronom. J.* 64(5):175-182, June 1959

12. Arp, H., "Southern Hemisphere Photometry VII; The Color-Magnitude Diagram of NGC 330 and the Adjoining Region of the Small Magellanic Cloud," *Astronom. J.* 64(7):254-258, September 1959

13. Chandrasekhar, S., "An Introduction to the Study of Stellar Structure," New York: Dover, 1957

14. Fowler, W. A., "Experimental and Theoretical Results on Nuclear Reactions in Stars. II," *Mém. Soc. Roy. Sciences de Liège,* cinquième série, 3:207-223, 1960

15. Salpeter, E. E., "Nuclear Reactions in Stars. Buildup from Helium," *Phys. Rev.* 107(2):516-525, July 15, 1957

16. Hayashi, C., Nishida, M., Ohyama, N., and Tsuda, H., "Stellar Synthesis of the α-Particle Nuclei Heavier than Ne^{20}," *Prog. Theoret. Phys.* 22(1):101-127, July 1959

17. Reeves, H., and Salpeter, E. E., "Nuclear Reactions in Stars. IV. Buildup from Carbon," *Phys. Rev.* 116(6):1505-1516, December 15, 1959

18. Sandage, A. R., and Schwarzschild, M., "Inhomogeneous Stellar Models. II. Models with Exhausted Cores in Gravitational Contraction," *Astrophys. J.* 116(3):463-476, November 1952

19. Härm, R., and Schwarzschild, M., "Numerical Integrations for the Stellar Interior," *Astrophys. J., Suppl. Ser.* 1(10):319-430, March 1955

20. Hayakawa, S., Hayashi, C., Imoto, M., and Kikuchi, K., "Helium Capturing Reactions in Stars," *Prog. Theoret. Phys.* 16(5):507-527, November 1956

21. Weymann, R., "I. Physical Conditions in the Circumstellar Envelope of α-Orionis and II. Comments on Mass Ejection Mechanisms in Red Giants," Mt. Wilson and Palomar Observatories Spec. Tech. Rept. No. 4, Carnegie Institution of Wash., Calif. Inst. Tech., Pasadena, Calif., Contract AF 49(638)-21, 1961

22. Gove, H. E., Litherland, A. E., and Clark, M. A., "Production of Neon in Stars," *Nature* 191(4796):1381-1382, September 30, 1961

23. Chiu, H.-Y., and Morrison, P., "Neutrino Emission from Black-Body Radiation at High Stellar Temperatures," *Phys. Rev. Letters* 5(12):573-575, December 5, 1960

24. Chiu, H.-Y., and Stabler, R. C., "Emission of Photoneutrinos and Pair Annihilation Neutrinos from Stars," *Phys. Rev.* 122(4):1317-1322, May 15, 1961

25. Chiu, H.-Y., "Annihilation Process of Neutrino Production in Stars," *Phys. Rev. Letters* 6(11):660, June 1, 1961

26. Artyukhina, N. M., and Kholopov, P. N., "Distribution of Stars in the Region of the Double Stellar Cluster h and χ Persei," *Soviet Astronomy, AJ* 3(6):923-936, May-June 1960

27. Sharpless, S., "The Distribution of M-Type Supergiants: I. Red Supergiants Near h and χ Persei and 30 Doradus," *Publ. Astronom. Soc. Pacific* 70(415):392-398, August 1958

28. Johnson, H. L., and Morgan, W. W., "Photometric and Spectroscopic Observations of the Double Cluster in Perseus," *Astrophys. J.* 122(3):429-433, November 1955

29. Johnson, H. L., "Intrinsic Colors of Early Type Stars," *Lowell Obs. Bull.* 4(2):37-46, August 1958

30. Arp, H. C., "The Hertzsprung-Russell Diagram," in: "Handbuch der Physik," S. Flügge, ed., 51:75-133, Berlin: Springer-Verlag, 1958

31. Oosterhoff, P. T., "A Study of the Double Cluster in Perseus, Based on Photographic Magnitudes and Effective Wavelengths Derived from Plates Taken by E. Hertzsprung at the Potsdam and Mount Wilson Observatories," in: Annalen van de Sterrewacht te Leiden 17, Part 1, 1937 (entire volume by author)

32. Sandage, A., "Observational Approach to Evolution. I. Luminosity Functions," *Astrophys. J.* 125(2):422-434, March 1957

33. van Maanen, A., "Investigation on Proper Motion. XXIII. The Proper Motion of the Cluster h Persei," *Astrophys. J.* 100(1):31-54, July 1944

34. Johnson, H. L., and Hiltner, W. A., "Observational Confirmation of a Theory of Stellar Evolution," *Astrophys. J.* 123(2):267-277, March 1956

Appendix A

Energy Generation Equations for the Carbon and Neon Burning Phases

Carbon and Neon Burning Near the Stellar Center

In general the rate of energy generation per gram may be expressed as

$$\epsilon = \epsilon_o \rho^{\alpha} T_9^{s} , \tag{A1}$$

where $\alpha = 1$ (carbon burning) and $\alpha = 0$ (neon burning).

Equations 10 and 11 of the text give the values of ϵ_o and s:

$$\epsilon_o = 1.0 \times 10^7 \, X_c^2 , \quad s = 33.3 \text{ (carbon burning);} \tag{A2}$$

$$\epsilon_o = 6.0 \times 10^3 \, X_{Ne} , \quad s = 65.2 \text{ (neon burning).} \tag{A3}$$

For the cases considered $X_c = 1.0$ and $X_{Ne} = 1.0$. The overall rate of energy generation is

$$\begin{aligned} L &= M\epsilon_c \int \frac{\epsilon}{\epsilon_c} dq \\ &= M^*\epsilon_c \frac{(1 - \beta_c)^{\frac{1}{2}}}{\beta_c^2} \int \left(\frac{\rho}{\rho_c}\right)^{\alpha+1} \left(\frac{T}{T_c}\right)^{s} x^2 \, dx , \end{aligned} \tag{A4}$$

where

$$\left.\begin{aligned} M^{*2} &= \frac{3}{4\pi a G^3} \left(\frac{k}{\mu_c H}\right)^4 ; \\ x^2 &= \frac{4\pi a G}{3} \left(\frac{\mu_c H}{k}\right)^2 \frac{\beta_c^2}{1 - \beta_c} T_c^2 r^2 . \end{aligned}\right\} \tag{A5}$$

Further computation shows that the above integral may be represented as

$$\begin{aligned} I &= \int_0^1 x^2 \exp\left\{-\frac{x^2}{6}\left[Cs + (\alpha + 1) D\right]\right\} dx \\ &\approx \left[\frac{6}{Cs + (\alpha + 1) D}\right]^{\frac{3}{2}} \frac{\sqrt{\pi}}{4} , \end{aligned} \tag{A6}$$

where

$$C = \frac{1}{(n+1)_c}$$

$$= \frac{8 - 6\beta_c}{32 - 24\beta_c - 3\beta_c^2} , \tag{A7}$$

and

$$D = \frac{1 - 4C}{\beta_c} + 3C$$

$$= \frac{24 - 21\beta_c}{32 - 24\beta_c - 3\beta_c^2} . \tag{A8}$$

Further reduction and substitution give the energy generation equation sought for the cases under consideration:

$$\frac{L_{core}}{L_\odot} = 0.2599 \frac{\epsilon_c}{\mu_c^2} \frac{(1 - \beta_c)^{\frac{1}{2}}}{\beta_c^2} \left[\frac{6 (n+1)_c}{s + (\alpha+1) N_c}\right]^{\frac{3}{2}} , \tag{A9}$$

where

$$N_c = \frac{D}{C}$$

$$= \frac{24 - 21\beta_c}{8 - 6\beta_c}$$

$$= \frac{3}{2}\left(\frac{1 + 8y_c}{1 + 4y_c}\right) . \tag{A10}$$

Helium Burning in a Shell

From Equation 6 of the text together with $dL(r)/dr = 4\pi r^2 \rho\epsilon$ and the approximations made by Hoyle and Schwarzschild*, the energy generation which is due to helium burning in a shell is found to be

$$L_{3\alpha, shell} = \epsilon_o \rho_{2e}^3 Y_{2e}^3 \left(\frac{T_2}{T_o}\right)^s \frac{4\pi r_2^3}{V_{2e}\left[3 + \frac{s-3}{(n+1)_{2e}}\right] - 3} . \tag{A11}$$

*Hoyle, F., and Schwarzschild, M., "On the Evolution of Type II Stars," *Astrophys. J., Suppl. Series* 2(13):8, June 1955.